Modeling the dynamics of sediment transport and resuspension in the northern Adriatic Sea

X. H. Wang

School of Geography and Oceanography, University College, Australian Defence Force Academy, University of New South Wales, Canberra, ACT, Australia

N. Pinardi

Corsodi Scienze Ambientale, Bologna University, Revenna, Italy

Received 15 January 2002; revised 19 July 2002; accepted 28 August 2002; published 21 December 2002.

[1] A coupled Adriatic Sea General Circulation and sediment transport model was used to study the dynamics of coarse and fine sediment transport and resuspension in the Northern Adriatic Sea. The sediment sizes of coarse (>50 μm) and fine (<50 μm) materials were sorted by their settling velocities. The bottom boundary layer (BBL) was discretized by a vertical sigma coordinate system with high resolution, and the wave-current interaction mechanism was considered. The sediment distributions and fluxes under various forcing conditions such as the Po River plume, the Bora and Scirocco wind stress and the surface waves were studied by process oriented numerical simulations. The conclusions are that maximum northward sediment transport occurs under the forcing by the Po River plume with the Scirocco wave resuspension. The largest southward sediment transport was due to the combined effect of the Po River plume and the Bora wind-forcing under the Bora wave conditions. A realistic forcing numerical experiment was also conducted for November 1994 when the full range of forcing functions were experienced by the region. This study shows that wave-driven sediment resuspension is an important resuspension mechanism in the shallow coastal areas of the Northern Adriatic Sea, and contributes significantly to the complexity of the sediment distribution and flux features in the region. *INDEX TERMS:* 4211 Oceanography: General: Benthic boundary layers; 4255 Oceanography: General: Numerical modeling; 4558 Oceanography: Physical: Sediment transport; *KEYWORDS:* sediment transport and resuspension, Adriatic Sea, bottom boundary layer, wave current interaction, numerical modeling, Po River plume

Citation: Wang, X. H., and N. Pinardi, Modeling the dynamics of sediment transport and resuspension in the northern Adriatic Sea, *J. Geophys. Res.*, *107*(C12), 3225, doi:10.1029/2001JC001303, 2002.

1. Introduction

[2] Studies on sediment transport in coastal oceans are fundamental to the future depiction of an integrated coastal management system. It is evident that marine sediments are the carriers for pollutants and nutrients from land sources, thus a good understanding of sediment movements are essential to control pollution and preserve ecology of coastal marine system [e.g., *Frascari et al.*, 1988; *Giordani et al.*, 1992]. On the other hand, coastal sediment dynamics involves sediment resuspension and deposition processes that can have severe adverse impact on recreational and maritime activities [*Warren and Johnsen*, 1993]. Recent studies on pelagic biomass growth in the Adriatic also shows that sediments in suspension at the sea surface can strongly hinder sunlight penetration into the water column, therefore affect the growth of phytoplankton at the subsurface [*Vichi et al.*, 1998].

0148-0227/02/2001JC001303$09.00

[3] There are essentially two physical processes that control sediment transport in coastal oceans. The first one is advection which transports suspended sediment materials (SSM) away from the input sources such as rivers. The other process is sediment resuspension at the sea bottom that provided sediment fluxes in to the water column. This vertical sediment transport is controlled by sediment settling and vertical motion of the water particles. It is also governed by vertical diffusivity generated by the turbulence in the boundary layers where velocity shear is strong due to the presence of skin friction. Wave current interaction further enhances the bottom resuspension in the bottom boundary layer (BBL), and can play an important role in the sediment transport in shallow waters.

[4] Studies of the SSM transport in the Northern Adriatic Sea have been conducted by many researchers [e.g., *Brambati et al.*, 1973]. However, these studies have remained at a level of sedimentological description and have not provided dynamic explanation to the sedimentological features observed in this region.

[5] This paper uses an Adriatic Sea General Circulation Model (ASGCM) coupled to a sediment transport model in

order to study the dynamics of the SSM transport in the Northern Adriatic Sea. The ASGCM is based on the three dimensional Princeton Ocean Model [*Blumberg and Mellor*, 1987] which uses a seabed following sigma coordinate system. The advantage of a sigma coordinate system ocean circulation model is that it is capable of resolving the BBL so that the BBL dynamics can be accurately represented in the simulation [*Zavatarelli and Mellor*, 1995; *Mellor and Wang*, 1996]. The sediment resuspension/deposition processes are parameterized following *Ariathurai and Krone* [1976]. We also considered a full wave-current interaction in the modeling of the BBL dynamics in order to examine the wave effect on the bottom stress and sediment resuspension. The paper uses process studies and a realistic simulation to quantitatively assess the sediment transport and resuspension processes under various forcing conditions existing in the region. Some model simulated features are compared with observed sedimentological characteristics in the Northern Adriatic Sea.

[6] In the next section, physical and sedimentological background is discussed for the Northern Adriatic Sea. Section 3 describes the ASGCM, sediment transport and resuspension/deposition model and wave-current interaction parameterization. Model results are described in section 4, and a final section offers discussions and conclusion of the paper.

2. Physical and Sedimentary Background

2.1. Physical Oceanography

[7] The Adriatic Sea general circulation has been studied recently both from data [*Artegiani et al.*, 1997a, 1997b] and model simulations [*Malanotte-Rizzoli and Bergamasco*, 1983; *Zavatarelli et al.*, 2002]. The general circulation is cyclonic and highly variable with seasons. The surface temperature excursion between summer and winter is more than 15°C and the net annual mean water balance is positive due to the river runoff contribution while the annual mean heat budget is negative due to the large winter heat losses in the Northern Adriatic. The meteoclimatology of the area presents strong northeasterly winds during winter, called Bora, while during summer and autumn winds are generally southeasterly at smaller amplitude (Scirocco). The large-scale wind- and thermohaline-driven currents experience large seasonal excursions due to all these forcing variabilities.

[8] One of the major features of the circulation is the boundary intensified current along the western side of the basin, the Western Adriatic Coastal Current (WACC). The latter is both wind and thermohaline driven. The WACC reaches maximum amplitude during winter due to the strong wind energy input but persists throughout the year, breaking into several baroclinic jets during the other seasons [*Poulain*, 2001]. The thermohaline structure of the WACC is connected to the Po fresh water river run-off [*Kourafalou*, 1999; *Raicich*, 1996]. The position of the WACC is controlled by bottom boundary layer processes which allow the current to shift from the western shelf areas in winter to the continental shelf slope during summer.

[9] The Northern Adriatic Sea is the shallower part of the Adriatic Sea (Figure 1b) and it shows an extended and gentle slope following the basin axis but a much higher continental slope gradient along the basin western side. The water masses of the Northern Adriatic are renewed every year and the densest waters slide down toward the deeper parts of the basin, composing the bottom waters of the middle Adriatic basin. During spring and summer the northern basin warms up from top to bottom and a well-defined seasonal thermocline forms. The seasonal pycnocline is large due to the additional contribution of the river run-off. The Po River discharges at an annual average rate of 1700 $m^3 s^{-1}$ and it is a fundamental controlling factor on the basin hydrodynamics and the WACC [*Kourafalou*, 1999].

[10] The basin long-term meridional circulation is anti-estuarine due to the dense water formation processes occurring in the Northern Adriatic Sea during winter. The thermal balance of the basin is maintained by a net inflow of heat at the Otranto Strait (see Figure 1a) which also give rise to the northward branch of the meridional transport cell. The WACC is part of the southward return branch which brings dense waters during winter and surface shelf waters during the other seasons toward the southern parts of the basin.

2.2. Sedimentology

[11] In the Northern Adriatic Sea, two main classes of sediments can be identified [*Brambati et al.*, 1973]. The first class consists of coarser sediments of sand with grain size between 50–2000 μm. The second class is of finer materials of silt with grain size between 2–50 μm. The finest class of clay sediment (<2 μm) can also be observed, but is not considered to be a major contribution in the fine sediment distribution of the Northern Adriatic Sea. In this study we consider only two types of sediments, namely the coarse component (>50 μm) and the fine component (<50 μm) of sediments.

[12] According to *Brambati et al.* [1973], fine sediments such as silt and clay are mainly supplied from the Northern Adriatic Sea rivers. They are transported in suspension by rivers to the sea and successively spread by ocean circulation. Since the general circulation of the Northern Adriatic Sea is cyclonic, and dominated by the WACC along the Italian coast, it is argued that the SSM from the northern rivers are transported southward by the coastal current. During this process, the SSM are mechanically sorted out by their grain sizes through the sediment deposition. Figures 4–6 of *Brambati et al.* [1973] show that the sorting mechanism is such that the sediment grain size decreases as the distance increases southward from the river sources.

3. Model Description

3.1. Adriatic Sea General Circulation Model

[13] The ASGCM is basically the Princeton Ocean Model (POM) implemented with an irregularly spaced grid in the whole Adriatic Sea [*Zavatarelli et al.*, 2002]. The horizontal resolution is about 3 km in the Northern Adriatic and about 10 km at the Strait of Otranto (Figure 1a). The model time steps are 20 s and 1000 s for external and internal modes respectively. The model has 21 sigma coordinate levels in vertical distributed logarithmically in the bottom and sur-

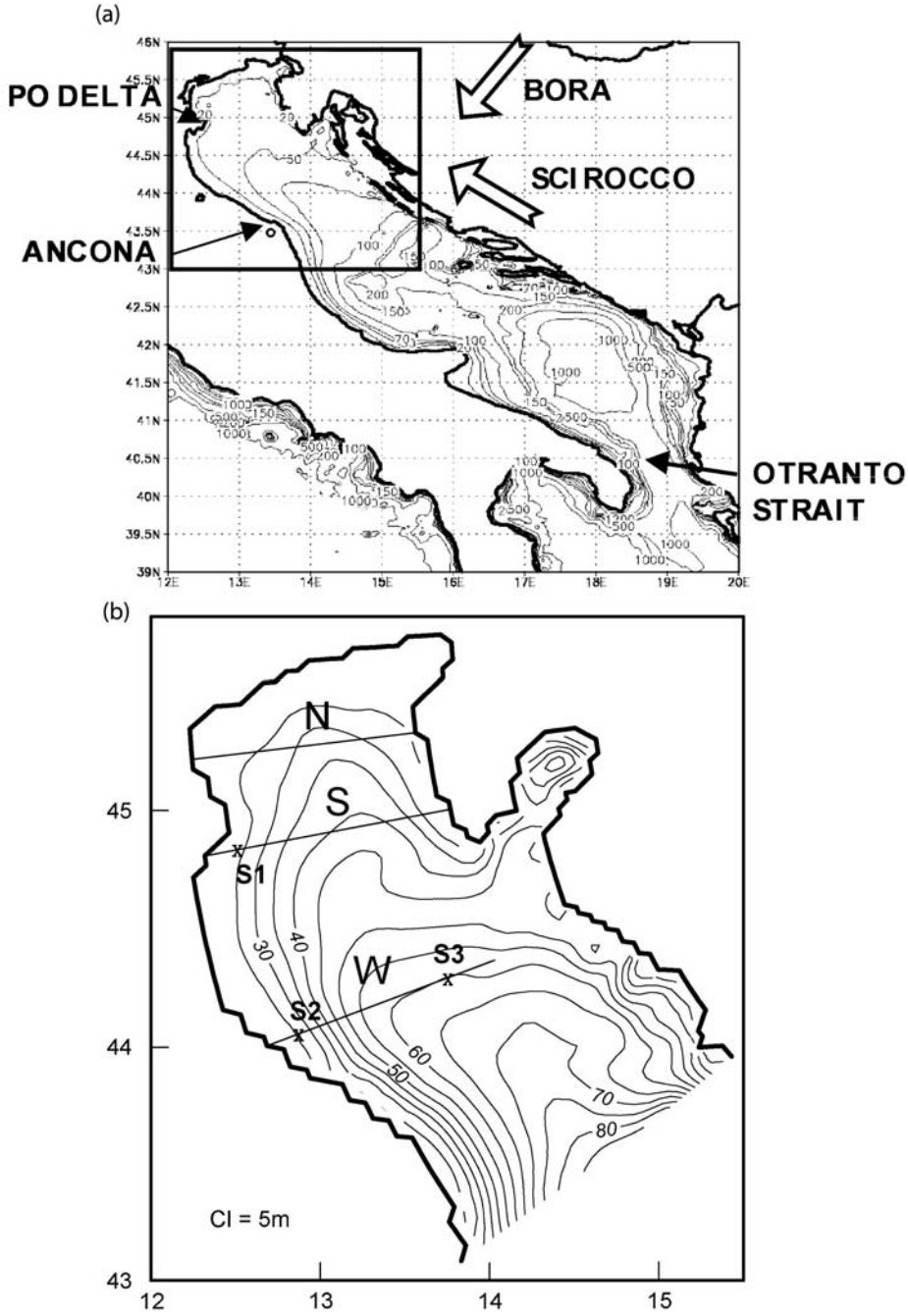

Figure 1. (a) Adriatic Sea General Circulation Model domain and the Adriatic Sea bathymetry with the directions of Bora and Scirocco winds denoted. (b) Submodel domain of the Northern Adriatic Sea. S1, S2 and S3 denote locations for station S1, S2 and S3, respectively. N, S and W denote three cross-sections north and south of the Po River delta, and on the western shelf, respectively.

face boundary layers to increase resolution there. In the shallow Northern Adriatic and along the western shelf areas, the BBL is resolved by a set of levels less than a meter thick for the bottom 10 m of the water column. The model uses the conventional 2.5 Mellor-Yamada turbulence closure submodel [*Blumberg and Mellor*, 1987] and Smagorinsky horizontal viscosity parameterization [*Smagorinsky*, 1963]. A detailed description of the model is given by *Zavatarelli et al.* [2002].

[14] At the model bottom level, the traditional bottom stress formulation is used which consists of

$$K_m\left(\frac{\partial \boldsymbol{u}}{\partial z}\right)_{z=-H} = \boldsymbol{\tau}_b/\rho \tag{1a}$$

where K_m is the vertical eddy viscosity coefficient calculated by the Mellor-Yamada submodel and is usually

due to the mean currents only and expressed as

$$\boldsymbol{\tau_b} = \rho C_d |\boldsymbol{u_b}| \boldsymbol{u_b} \tag{1b}$$

where

$$C_d = Max\left\{ \left[\frac{1}{\kappa} \ln(H + z_b)/z_0 \right]^{-2}, 0.0025 \right\}. \tag{1c}$$

Here κ is the Von Karman constant, H is the total water depth, z_0 is the bottom roughness set equal to 0.001 m and $\boldsymbol{u}_b$ is the bottom ($z = z_b$) mean current velocity field. This parameterization will be changed and z_0 will be modified if wave-current interaction processes are considered as explained in section 3.2.

[15] In this paper, we use the model for two different sets of numerical experiments. The first set of experiments consists of process oriented studies in order to assess the sediment fluxes and distributions under various forcing conditions observed for the Northern Adriatic Sea. In the second set of experiment, the ASGCM has been run with realistic wind stress, surface heat flux and river runoffs forcings continuously from 1992 to 1994. The sediment transport model has been coupled to this ASGCM experiment starting from October 31, 1994. The model is run for November 1994 where all forcing parameters including wave data for SSM transport model were available. November 1994 is also a very anomalous river runoff year where the Po flooded and gave runoff values as high as 9000 m^3 s^{-1} for a few days, as shown later. We therefore have a particular interest in examining sediment transport caused by lateral advection under such strong ambient buoyancy forcing conditions.

3.2. Wave-Current Interaction

[16] In the shallow regions of the Adriatic Sea, the combined effect of the surface waves and mean circulation on the bottom stress, and thus on the sediment resuspension, may be significant. The important advancement of wave-current interaction theory is due to *Grant and Madsen* [1979, 1986]. The concept of their work is that the nonlinear interaction of the surface waves and currents enhances the shear stress in a much thinner wave boundary layer that exists inside of the mean current BBL. This enhancement of the bottom stress is mainly caused by an apparent increase in the bottom roughness z_0 (apparent roughness) due to the wave-generated turbulence in the wave boundary layer. Some effects of the waves on the bottom stress are also felt by the contribution of the oscillatory wave flow to the total current in that layer. Moreover, according to *Eidsvik* [1993], the wave contribution of the turbulence production above the wave boundary layer is negligible as the wave orbital velocity shear is small there. Therefore the mean flow BBL hydrodynamics is only affected by the waves for an increased bottom roughness and thus an increased drag coefficient C_d.

[17] Based on the wave-current interaction model of *Grant and Madsen* [1979], the bottom stress amplitude $|\tau_b|$ can be parameterized by using a modified bottom stress quadratic drag law and a wave-current friction factor f_{cw},

$$|\tau_b| = \frac{1}{2} f_{cw} \rho |\boldsymbol{u}_b + \boldsymbol{u_w}|^2 \tag{2}$$

where $|\boldsymbol{u}_b|$ is the mean bottom current and $|\boldsymbol{u}_w|$ is the bottom wave orbital velocity. The mean current used here is calculated by the ASGCM.

[18] In equation (2), $|\boldsymbol{u}_w|$can be computed by a linear wave theory for given wave height h_s and period T_s:

$$|\boldsymbol{u}_w| = 0.5 h_s \omega / \sinh(kH) \tag{3}$$

and

$$\omega^2 = gk \tanh(kH) \tag{4}$$

where $\omega = 2\pi/T_s$ and k is the wave number.

[19] The determination of the bottom roughness z_0 and wave-current friction factor f_{cw} involves an implicit Kelvin function with two inputs: the ratio of bottom roughness to the wave excursion at the seabed, and the ratio of mean current and wave orbital velocity at the sea bottom. For given waves with $\boldsymbol{u}_w$ determined by equations (3) and (4), z_0, f_{cw} can be calculated by an iterative procedure described by *Lou et al.* [2000].

[20] In our study, we assumed that $\boldsymbol{u}_b$ and $\boldsymbol{u}_w$ are in the same direction so that a maximum bottom stress due to wave current interaction was used in the sediment transport model. A similar simplification was made by *Jewell et al.* [1993] in their study of sediment distribution on the Amazon continental shelf. Because the tide induced bottom stress is significantly less than wave induced bottom stress and the tidal residual currents are negligible in the Northern Adriatic Sea, the tidal currents are excluded in this study.

3.3. Sediment Transport Model

[21] The sediment transport model used here was similar to that of *Ribbe and Holloway* [2001] for their study on the suspended sediment transport by internal tides in Australian Northwest shelf. The model has been improved to include wave current interaction mechanism for sediment resuspension in shallow water systems. *Wang* [2001] applied the model to Jervis Bay, New South Wales, Australia, to study sediment flux and distribution due to winter storms. Several assumptions have been made. We first assumed that the SSM do not flocculate or aggregate so that the SSM in the water column are noncohesive and the sediment mixture behaves as a Newtonian fluid. For sediments such as fine sand and silt ($20 < d < 60$ μm), we also assumed that the sediment resuspension is supported by turbulence, and horizontal advection plays an equally important role in determining the SSM concentration as that of resuspension. Furthermore, we neglected the inertia of the SSM particles so that their vertical velocity differs from that of water by a small constant settling velocity w_s. Finally, we assume that the SSM concentrations have no effects on the water density. This assumption can only be applied to an environment where the SSM concentrations are small. In a highly turbid environment ($C > 1$ kg m^{-3}), the resuspended sediments can stratify the BBL thus the above assumption will become invalid [e.g., *Adams and Weatherly*, 1981; *Trowbridge and Kineke*, 1994; *Fohrmann et al.*, 1998]. The validity of this assumption will be examined later.

[22] The three-dimensional equation describing the SSM transport is based on the conservation of the SSM in the

water column for an incompressible flow,

$$\frac{\partial C}{\partial t}+\frac{\partial}{\partial x}(uC)+\frac{\partial}{\partial y}(vC)+\frac{\partial}{\partial z}[(w+w_s)C]=\frac{\partial}{\partial z}\left(K_h\frac{\partial C}{\partial z}\right)+F_C \tag{5}$$

where x, y, z, u, v, w represent zonal, meridional and vertical (positive upward) coordinates and their velocity projections, C is the SSM concentration (g m^{-3}), K_h is vertical eddy diffusivity coefficient for the SSM which was assumed to be equal to that of heat and salt, and is calculated by 2.5 Mellor-Yamada turbulence closure scheme. F_C is the horizontal diffusion term for C parameterized according to *Smagorinsky* [1963].

[23] As the SSM particle velocity only differs from the water velocity by w_s in the vertical direction, the settling velocity value (w_s) is not changed in equation (5) after its conversion into a σ-coordinate system. For an interested reader, the transformation of w_s into a σ-coordinate system can be reviewed in the Appendix. We used two sets of equations like equation (5) concomitantly in the model: one for the coarse sediment material (CSM) and the second for the fine sediment material (FSM).

[24] According to *Frascari et al.* [1988], an annual supply of 20 Mt yr^{-1} of sediment comes from rivers surrounding Adriatic Sea. The Po River accounts for 70% of the total budget. Therefore, the net sediment flux at the sea surface was prescribed to this annual discharge of sediment S_r. Seventy percent of the flux was distributed at the Po River mouth represented by six coastal nodes, and the rest was equally distributed at the other rivers or land drainage areas along the Adriatic coast represented by point or line sources. Thus we have

$$K_h\frac{\partial C}{\partial z}=S_r \qquad \text{at} \qquad z=\eta \tag{6}$$

for each river. The sediment discharges carried equal load of the CSM and the FSM components.

[25] At the sea bottom, sediment concentration gradient was prescribed according to

$$K_h\frac{\partial C}{\partial z}=S \qquad \text{at} \qquad z=-H \tag{7}$$

where S is the net sediment flux normal to the bottom boundary due to deposition or resuspension at the seabed. According to *Ariathurai and Krone* [1976], the seabed sediment flux S can be formulated as following

$$S=\begin{cases} S_0\left(\frac{|\tau_b|}{\tau_c}-1\right) & \text{if} |\tau_b|>\tau_c \\ C_b w_s\left(\frac{|\tau_b|}{\tau_c}-1\right) & \text{if} |\tau_b|<\tau_c. \end{cases} \tag{8}$$

[26] Here S_0 is an empirical constant and was set to 10^{-4} kg m^{-2} s^{-1} [*Clark and Elliot*, 1998]. A constant S_0 also implies that there is an indefinite source for sediment resuspension at the seabed. C_b is the suspended sediment concentration at the model bottom layer. Bottom stress τ_b was normally computed by equation (1b). However, equation (2) was used when there were waves.

[27] The SSM transport model was run concurrently with the hydrodynamic model with same internal time step given above. The model numerical scheme is similar to that used for solving scalar variables such as salinity and temperature in POM [*Mellor*, 1998]. The integration of equation (5) is carried out by two steps. The first step is to implicitly solve C due to vertical diffusion. The second step is to explicitly integrate C for advection and horizontal diffusion. The advection term is differenced according to either a central differencing scheme in the process study experiments or the three-iteration Smolarkiewicz upstream scheme [*Smolarkiewicz*, 1984] for the realistic forcing experiment. The latter scheme provided smoother solutions for sediment concentrations, with negligible changes in the depth averaged flux values. With 50% increase in computational overhead, the latter scheme has overcome some localized but severe overshooting in sediment concentrations encountered in the realistic simulation of November 1994 when the former scheme was used.

Table 1. Parameters for Sediment Transport Model

Parameter	Value
S_0 (kg m^{-2} s^{-1})	10^{-4}
ν (m^2 s^{-1})	1.3×10^{-6}
ρ_s (kg m^{-3})	1100
w_s (m s^{-1})	$-10^{-5} \sim -10^{-4}$
τ_c (N m^{-2})	0.02
$S_{r\text{Po}}$ (kg m^{-2} s^{-1})	3.4×10^{-6}

[28] The SSM transport model described by equations (5) through (8) involves parameters of settling velocity w_s, and critical stress τ_c for resuspension and deposition. Stokes law and Shields function were used to determine w_s and τ_c according to

$$w_s=\frac{gd^2}{18\nu}(\rho_s/\rho_w-1) \tag{9}$$

and

$$\tau_c=\rho_w\left[\frac{0.1g(\rho_s-\rho_w)\nu}{\rho_w}\right]^{2/3} \tag{10}$$

where d is sediment grain diameter and $\nu = 1.3 \times 10^{-6}$ m^2 s^{-1} is the molecular kinematic viscosity.

[29] For sediments such as fine sand and silt ($20 < d < 60$ μm) with a density $\rho_s = 1100$ kg m^{-3}, the settling velocity w_s ranges from -1×10^{-4} m s^{-1} to -1×10^{-5} m s^{-1} and τ_c is calculated to be 0.02 N m^{-2}. For easy reference, Table 1 lists the model parameters. These values are within ranges of those used by other researchers [e.g., *Adams and Weatherly*, 1981; *Clark and Elliot*, 1998; *Chao*, 1998; and *Kampf et al.*, 1999].

4. Model Results

4.1. Process Study Experiments

[30] The suspended sediment materials in Northern Adriatic Sea is either induced by river sources or resuspended from the seabed in response to various forcing conditions. To quantify the relative importance of these processes, we first performed several process study experiments to examine sediment fluxes and distributions. The model runs are either forced by Po River plume only (Experiment 1), or both Po River plume and the wind stress (Experiment 2). We conducted these experiments both without and with wave resuspension by means of wave current interaction (Experiment 3, 4 and 5). Winter mean values were used for

Table 2. Process Study Experiments With Their Forcing Functions and Model Predicted Total (FSM + CSM) Sediment Load Transported Across Cross-Sections N and S on day 30[a]

	Run	Po River Runoff ($m^3 s^{-1}$)	Wind Regimes	Wave Regimes	Total Sediment Transport (kg s^{-1})	
					Cross-section N	Cross-section S
Experiment 1	first	2000	No	No	132	−14
	second	4000	No	No	196	−39
	third	1000	No	No	143	−11
	fourth	2000[b]	No	No	229	−66
Experiment 2	first	2000	Bora	No	−147	−772
	second	2000	Scirocco	No	18	−201
Experiment 3	first	2000	No	Bora	141	−20
	second	2000	No	Scirocco	416	180
Experiment 4	first	2000	Bora	Bora	−176	−776
	second	2000	Scirocco	Scirocco	−322	−195
Experiment 5	first	2000	Bora	SMB Bora	−146	−760

[a]Negative value defines southward transport. "No" indicates an exclusion of the forcing function in the respective experiments.

[b]In this run, in addition to the Po River runoff all the other rivers were set to their climatological winter values for a total amount of fresh water discharge of 7200 $m^3 s^{-1}$.

the Po River runoff, and the climatological conditions were used for the wind stress and the wave forcing. Both climatological Bora and Scirocco wind stress are assumed to have equal magnitude of 0.1 N m^{-2}. Two wind vectors in Figure 1a show the directions of these winds. These forcing conditions are typical to the region [e.g., *Raicich*, 1996, *Artegiani et al.*, 1997a, 1997b; *Cavaleri and Bertotti*, 1997; *Kourafalou*, 1999] and are summarized in Table 2. The model was initialized by constant water temperature of 12°C and salinity of 38 psu, representing a winter ambient environment without stratification. All the experiments were started from rest and run for a period of 30 days with continuous Po River buoyancy forcing. At the model open boundary in the Ionian Sea, the explicit Orlanski radiation condition was used for water temperature, salinity and sediment concentrations, while the current velocity was set either to zero for buoyancy forcing runs or prescribed to the winter transport rates for wind-forcing runs.

4.1.1. Po River Plume, Without Waves

[31] The first model run in this experiment was forced by the Po River buoyancy input with a winter mean rate of 2000 $m^3 s^{-1}$ for the entire model period. A quasi-steady-state sediment plume was established after day 20, and total horizontal sediment transport normal to the cross sections N and S (Figure 1b) reached near constant values. The model simulated surface and bottom velocity fields on day 30 are shown in Figure 2 and are in agreement with the depiction of *Kourafalou* [1999] in their study of Po River plume dynamics. The plume-driven circulation was clearly baroclinic with southward coastal currents at the surface south of the Po River delta and a northward returning flow at the bottom. Due to the small bottom currents, the model simulated bottom stress was too weak to resuspend bottom sediments.

[32] Of particular interest is the surface anticyclonic gyre north of the delta produced by a balance between alongshore surface elevation gradient and Coriolis force there. This balance is possible due to a protruding coastline of the Po River delta. The detailed description of its development is given by *Kourafalou* [1999]. Figure 3 shows the depth averaged sediment fluxes and distributions for FSM and CSM on day 30. Owing to the northern plume gyre, northward transport of both FSM and CSM was evident near and north of the delta, and the sediment plumes was extended right to the northern coast of the Adriatic. Due to a faster settling rate, the CSM plume was mostly confined to the

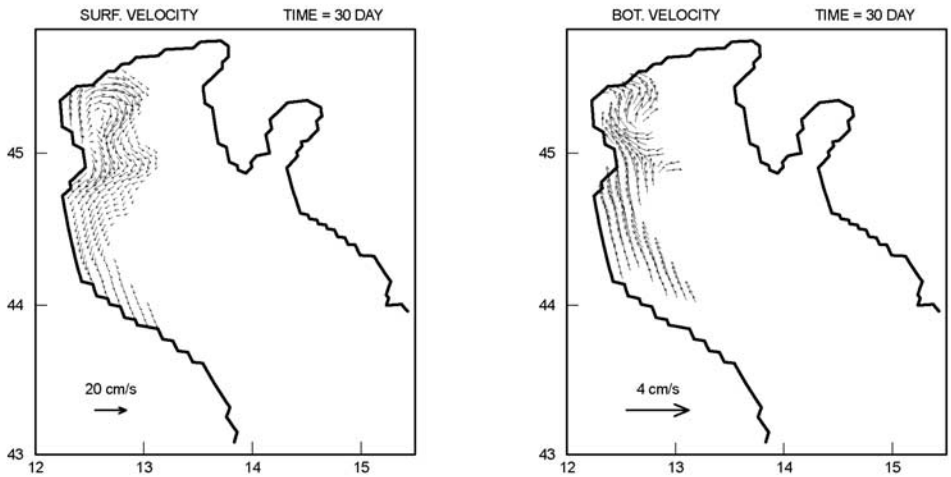

Figure 2. Model simulated (left) surface and (right) bottom velocity fields by the winter Po River plume forcing run (Experiment 1, Run 1 in Table 2). Vectors less than 10% of maximum velocity are not plotted.

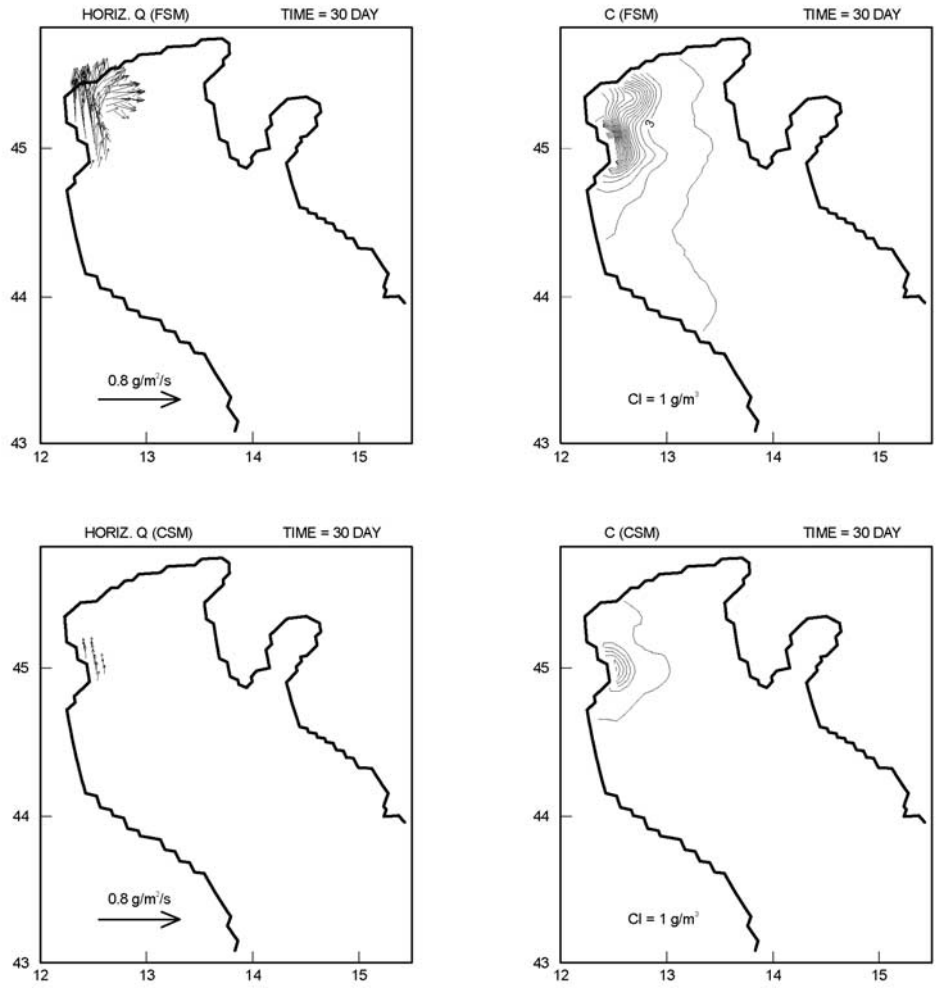

Figure 3. Same as Figure 2 but for the depth-averaged sediment fluxes and concentrations. Vectors less than 10% of maximum fluxes are not plotted.

sediment source, and the values of CSM concentration and flux are 4 to 5 times lower than those of the FSM plume. Similarly, as the FSM plume turned anticyclonically back toward the coast south of the delta, its concentration decreased along the sediment trajectories as well as the sediment flux.

[33] To examine the vertical structures of sediment distributions and fluxes, FSM and CSM concentrations and horizontal fluxes normal to the cross-section N are shown in Figure 4. For convenience we hereafter refer the positive (negative) flux as a northward (southward) sediment transport. High FSM concentration values were observed in two regions, with one at the surface near the Po delta and the other at the subsurface offshore. This pattern is a vertical manifestation of a slowly sinking sediment plume trapped in the northern anticyclonic plume gyre described earlier. Furthermore, the FSM flux was dominated by the velocity field and had maximum values at the surface for both a northward flux nearshore and a southward flux offshore. We note that at this cross-section, both CSM concentration and flux are negligible. The area integrated total (FSM + CSM) horizontal transport normal to the cross-sections N and S on model day 30 are listed in Table 2.

[34] To elucidate the effect of variability in Po River buoyancy forcing on the sediment processes, the second and third model runs were performed with Po River runoff rate either doubled or halved. The river sediment discharge rate in equation (6) remained the same as in the first run. While it is expected from the second run that the total sediment transport at both cross-sections were increased, the weaker hydrodynamical plume in the third run, consisting in particular of a weaker return flow in the northern plume gyre increased the total sediment transport at the cross-section N with respect to the first run (Table 2).

[35] For completeness, we conducted the fourth model run that considered the winter freshwater inputs from all 13 major rivers in the Adriatic Sea. The Po River runoff was maintained at the winter mean value and the Po River was the only sediment source. The rest of rivers give total runoffs of 5200 $m^3 s^{-1}$ that was equally distributed to these river sources. As the freshwater runoffs from northern rivers reduced the alongshore pressure gradient north of the Po River, the weakened northern plume gyre has again increased the northward sediment transport at the cross-section N. The strengthened southward coastal currents also increased southward sediment transport at the cross-section S (Table 2).

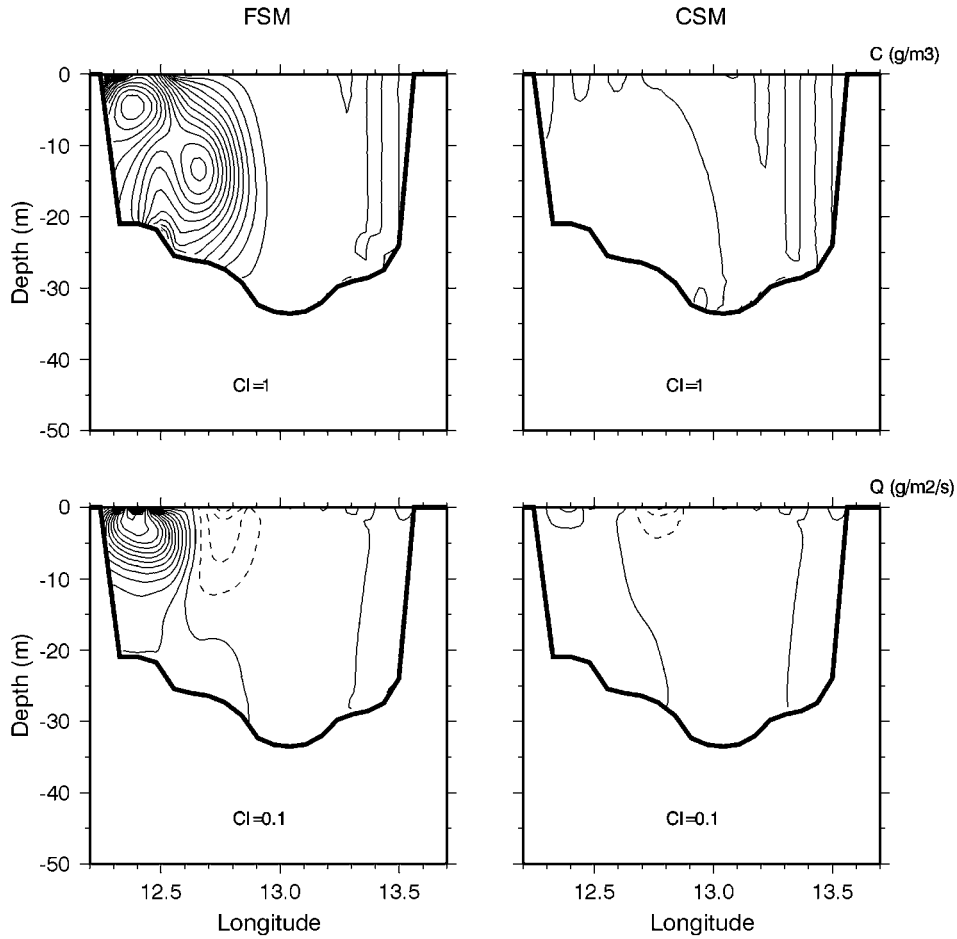

Figure 4. Model simulated day 30 (top) sediment concentrations and (bottom) fluxes at cross-section N by winter Po River plume forcing run (Experiment 1, Run 1 in Table 2). Southward fluxes are in negative values, denoted by the dashed lines.

4.1.2. Po River Plume With Wind Stress, Without Waves

[36] This experiment considers the wind effect on the Po River sediment plumes. The model was forced by the Po River winter runoff for 25 days. An either northeasterly "Bora" or a southeasterly "Scirocco" wind stress of 0.1 N m^{-2} was then added to the model forcing and the model runs were continued for 5 more days. Figure 5 shows model predicted surface velocity fields and bottom stress on day 30 for both Bora and Scirocco runs. As shown in the figure, the Bora wind strengthened the southward coastal currents associated with the Po River plume, while the Scirocco eliminated the plume coastal currents. Moreover, the anticyclonic gyre north of the Po delta was also removed under the forcings of both wind regimes. Higher bottom stress in the shallow coastal regions was also predicted. Moderate sediment resuspension consequently occurred there.

[37] Figure 6 shows the depth averaged sediment fluxes and concentrations from the Bora run. Enhanced southward coastal currents and the bottom sediment resuspension produced western shelf intensified FSM and CSM fluxes. The FSM plume extended southward almost as far as Ancona (13.5°E, 43.6°N), and the CSM plume was displaced further south of the Po delta with respect to Experiment 1. As the sediment flux is the production of SSM concentration and current velocity, a higher FSM concentration in the water column has led to a stronger FSM flux than that of CSM in the coastal regions between section S and W (Figure 1b).

[38] Figure 7 shows the depth averaged sediment fluxes and distributions from the Scirocco run. While the FSM plume was more displaced offshore owing to the upwelling favored wind forcing, the elimination of southward coastal currents confined the plume to the northern part of the basin. Both FSM and CSM show some low concentrations in coastal regions due to resuspension. Sediment flux patterns resembled a wind-driven two-dimensional circulation in a closed basin with down wind currents near the shallower coast and a returning flow in the deeper center. This pattern was modified by the Po River runoff near its river delta, where the predominant direction of both fluxes was to the south.

[39] Both Bora and Scirocco winds reversed or significantly reduced northward sediment fluxes at the cross-section N, and produced significant southward fluxes at the cross-section S. Table 2 shows the total sediment transport at both cross-sections.

4.1.3. Po River Plume With Surface Cooling

[40] During winter season the Northern Adriatic Sea experiences strong atmospheric cooling with surface heat loss as high as 500 W m^{-2} during Bora events [e.g., *Hendershott and Rizzoli*, 1976; *Artegiani et al.*, 1997b].

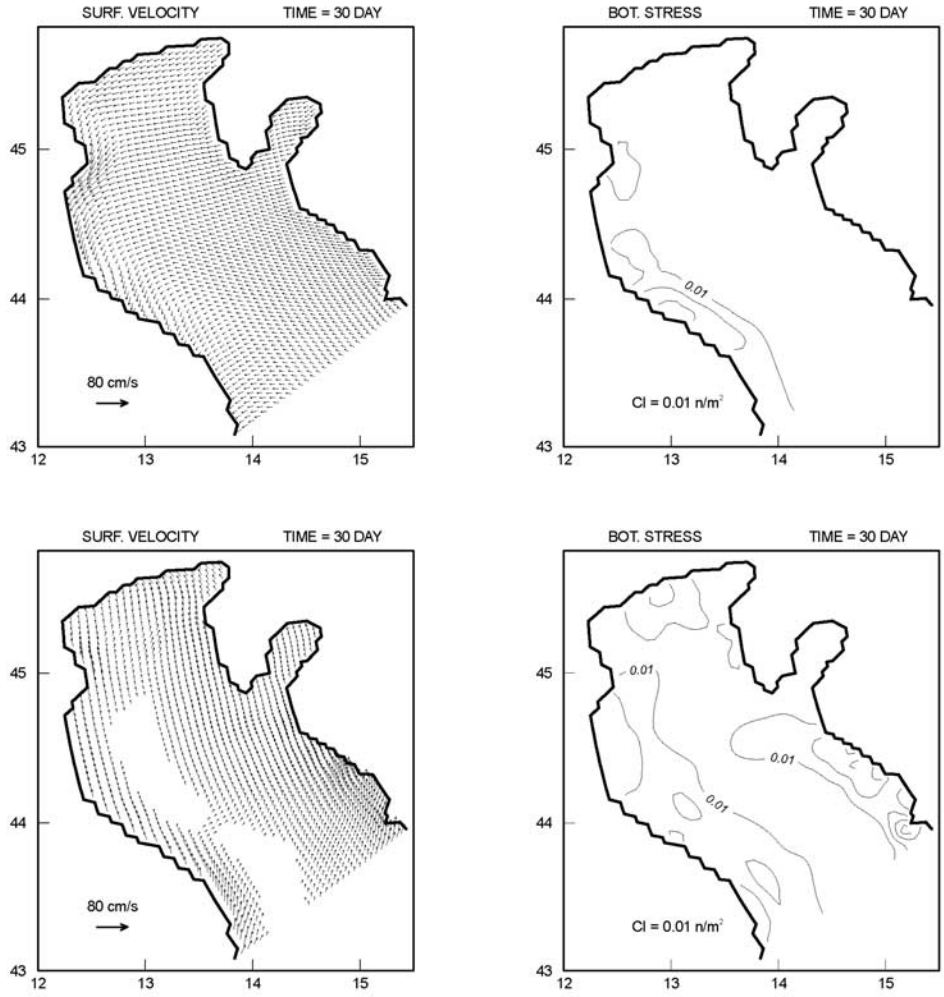

Figure 5. Model predicted surface velocity and bottom stress fields by the winter Po River plume and (top) Bora or (bottom) Scirocco wind-forcing runs (Experiment 2, Run 1 and 2 in Table 2). Vectors less than 10% of maximum velocity are not plotted.

In addition to the winter Po River runoff, a continuous surface heat loss of 200 W m^{-2} was imposed to the model surface boundary for entire modeling period. Unlike some smaller semienclosed basins such as Jerivs Bay in Australia where strong atmospheric cooling generates significant circulation [*Wang and Symonds*, 1999], differential cooling in the Northern Adriatic Sea resulted in negligible density currents at the surface (<0.05 m s^{-1}) owing to a gentle and broad slope of the northern shelf. Weak but more coherent bottom currents developed on the southern shelves where their slopes are increased and formed a cyclonic gyre there. However, no sediment resuspension occurred and the sediment fluxes and distributions predicted by this run are not changed from Figure 3.

4.1.4. Po River Plume, With Uniform Wave Fields

[41] Sediment fluxes and distributions due to wave resuspension were studied in this experiment using wave current interaction mechanism. Two spatially uniform wave regimes are considered. According to *Cavaleri et al.* [1997], Bora winds typically produce waves with significant wave height of 1 m, and period of 5 s. In contrast, Scirocco winds generate waves with typical height of 0.5 m and period of 10 s. The model was continuously forced by winter Po River runoff for 30 days, and considered wave current interaction mechanism for one day from day 29.

[42] Figures 8a and 8b are the model simulated bottom stresses on day 30 with Bora and Scirocco waves, respectively. Scirocco waves have longer wave period and produced much stronger bottom stress in the shallow coastal regions. In contrast, shorter period Bora waves generated moderate bottom stress that caused small amount of sediment resuspension in the region near the northern coast and the Po delta.

[43] Depth averaged sediment distribution and fluxes are shown in Figure 9 for Scirocco wave run. High sediment concentrations in the northwest coast produced high northward fluxes where plume-driven coastal currents were strong. The anticyclonic plume gyre north of the Po River again produced northward fluxes as in Figure 3. However, due to the wave resuspension there was a significant increase in CSM flux there. In the south of Po River delta, northward fluxes of both FSM and CSM were caused by the coupling effect of northward subsurface currents and bottom intensified sediment concentrations. As the CSM had larger

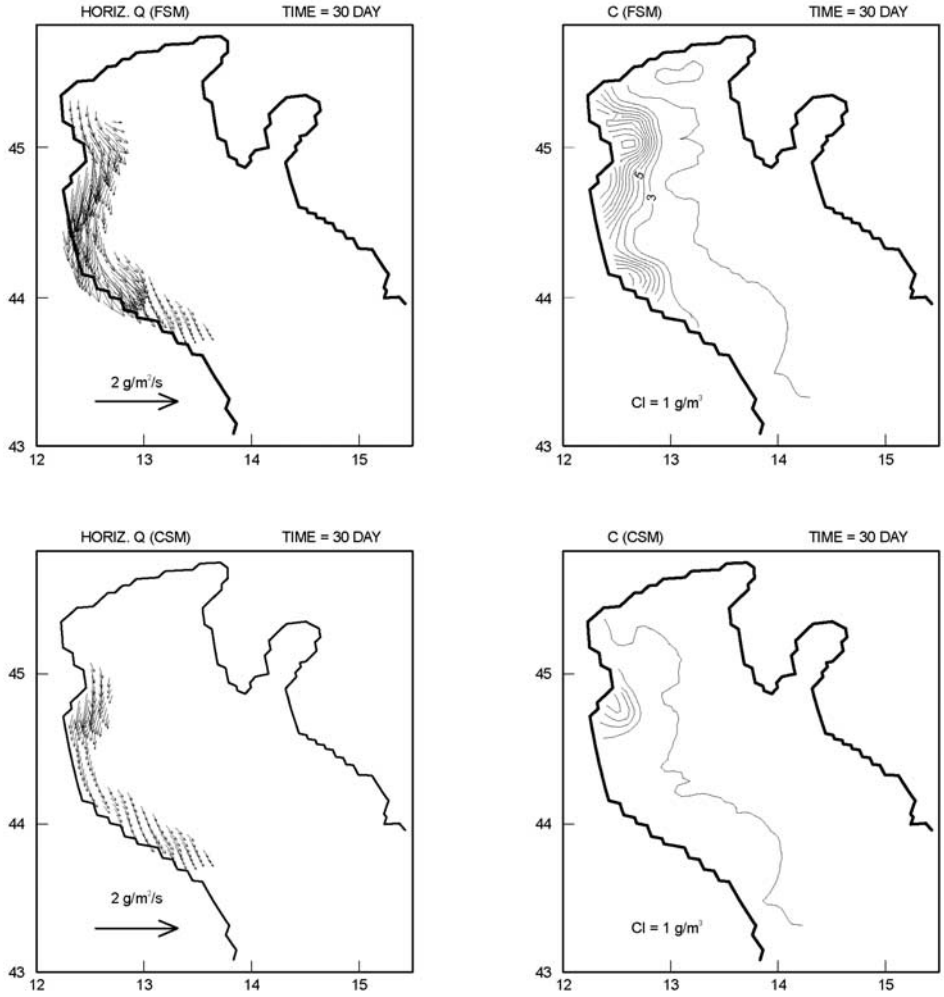

Figure 6. Model simulated depth averaged sediment fluxes and concentrations by the winter Po River plume and Bora wind-forcing run (Experiment 2, Run 1 in Table 2). Vectors less than 10% of maximum fluxes are not plotted.

near bottom concentration than that of the FSM, the CSM flux was stronger. We note that Scirocco wave run generated northward sediment flux at the cross-section S, and the total sediment transport at both cross-sections are listed in Table 2 for both runs.

4.1.5. Po River Plume With Wind Stress, and Uniform Wave Fields

[44] In this experiment, we repeated the previous experiment adding wind stress forcing for the last five days of the model runs. The respective depth averaged sediment flux and distribution patterns are similar to Figures 6 and 7. However, both horizontal sediment flux and concentration values were increased by the wave resuspension. Total sediment transport predicted by both runs is large and southward at both cross-sections. The rates of the total sediment transport are shown in Table 2.

4.1.6. Po River Plume With Wind Stress, and Sverdrup-Munk-Bretschneider Wave Fields

[45] The wave experiments conducted above used idealistic wave fields that had spatially uniform distribution of wave heights and periods. As rightly pointed out by one of the reviewers, this assumption may result in unrealistic sediment suspension and under-prediction of wind-driven currents due to the effect of the wave-current interaction.

[46] Using the third-generation WAM wave model, *Cavaleri et al.* [1989] and *Cavaleri and Bertotti* [1997] have predicted wave fields forced by both Bora and Scirocco storms in the Adriatic Sea. A Scirocco is a longshore wind that blows over all the Adriatic Sea, leading to a relatively mild long fetch wave generation or swell conditions in the Northern Adriatic Sea. Thus uniform waves fields were predicted there under the southeast winds. We concluded that using constant wave fields in the Scirocco wave experiments is a reasonable assumption for the Northern Adriatic Sea, and should not result in unrealistic sediment distributions and fluxes there.

[47] In contrast, a Bora wind is an onshore wind blowing over the Northern Adriatic Sea. The waves there are fetch-limited and purely generative. Therefore, the Bora wave fields in the Northern Adriatic are not uniform, and large cross-shore gradients were predicted for both wave heights and periods.

[48] To exam the effects of a spatially variable Bora wave fields on the sediment resuspension and wind-driven cur-

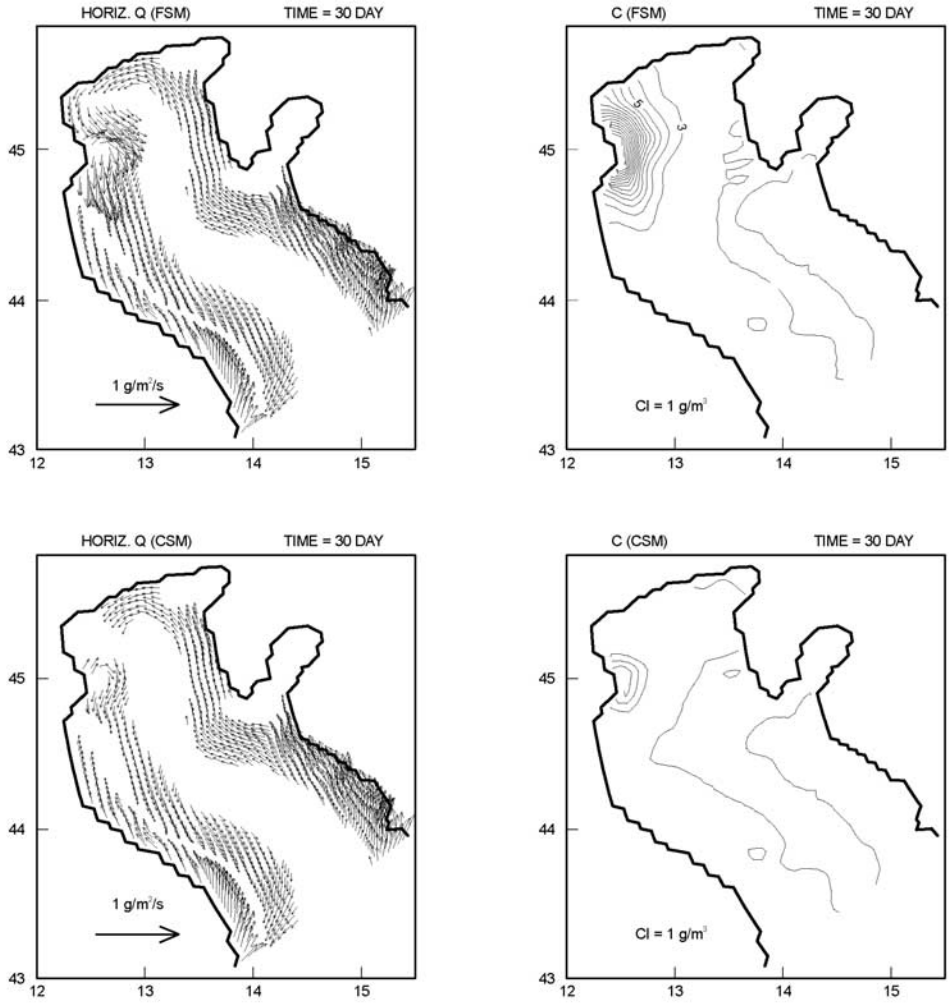

Figure 7. Same as Figure 6 but for Scirocco wind (Experiment 2, Run 2 in Table 2). Vectors less than 10% of maximum fluxes are not plotted.

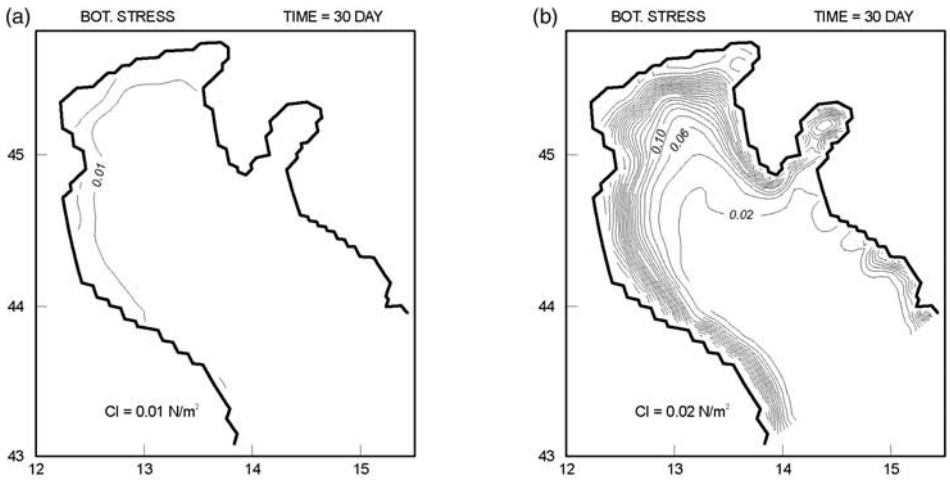

Figure 8. Model simulated bottom stress fields by the winter Po River plume and (a) Bora wave or (b) Scirocco wave forcing runs (Experiment 3, Run 1 and 2 in Table 2).

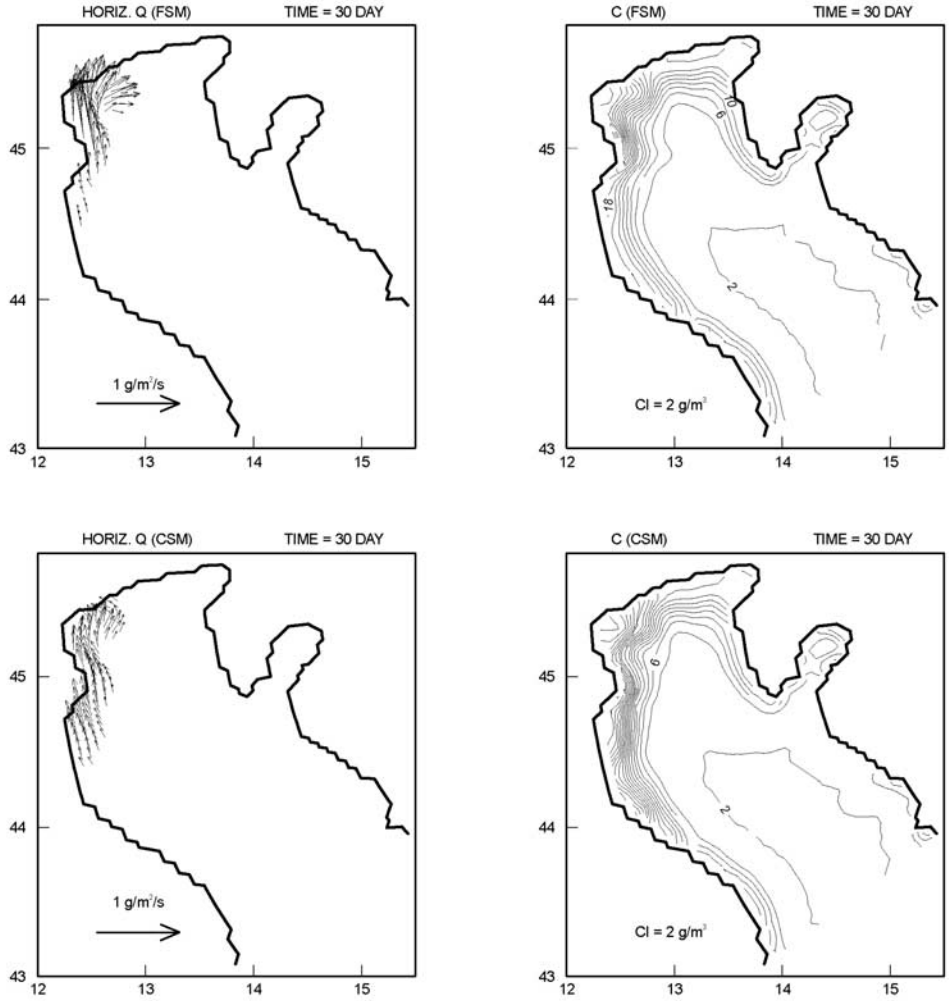

Figure 9. Model simulated depth averaged sediment fluxes and concentrations by winter Po River plume and Scirocco wave forcing run (Experiment 3, Run 2 in Table 2). Vectors less than 10% of maximum fluxes are not plotted.

rents, we repeated the previous experiment. The uniform Bora wave field has been replace by a more realistic wave field generated by the Sverdrup-Munk-Bretschneider (SMB) wave model [*Bretschneider*, 1970] under the forcing of a constant Bora wind of 8 m s^{-1} (wind stress of 0.1 Pa). The SMB wave hindcasting equations are

$$\frac{gh_s}{W^2} = 0.283 \tanh\left[0.0125\left(\frac{gX}{W^2}\right)^{0.42}\right] \tag{11}$$

$$\frac{gT_s}{W} = 7.54 \tanh\left[0.077\left(\frac{gX}{W^2}\right)^{0.25}\right] \tag{12}$$

where W is the wind speed and X is the fetch length.

[49] In the Northern Adriatic Sea with an average fetch of 110 km, the SMB wave height and period are increased from 0.4 m and 2.3 s at the eastern coast to 1.1 m and 4.2 s on the western shore, respectively. On the eastern shore, both uniform and SMB wave experiments predicted the bottom stress that is smaller than the critical stress for resuspension (e.g., Figure 8). The resuspended sediment concentrations are negligible from the both model runs. On the western shore, the SMB wave periods ($T_s \sim 4$ s) are smaller than that used in the uniform wave field experiment ($T_s = 5$ s), and resulted in a wave-induced bottom stress that also becomes less than the critical stress value for resuspension. Thus, the sediment distributions and fluxes on the western shore are no longer affected by the waves. Figure 10 shows the difference in the sediment concentrations and current velocity at the cross-section N between two experiments of the uniform and the SMB wave fields. The bottom FSM and CSM concentrations predicted the SMB wave run is reduced by up to 5 g m^{-3} on the western shore. The reduced bottom stress did not affect wind-driven currents, as also shown in Figure 10.

[50] Finally the total sediment transport at the cross-section N and S are listed in Table 2, and is compared with those predicted by the uniform Bora wave run. The southward sediment transport predicted by SMB wave experiment is reduced by 17% at the cross-section N and 2% at the cross-section S. The change in total sediment flux at the cross-section S was small as the Po River sediment plume dominated the transport there.

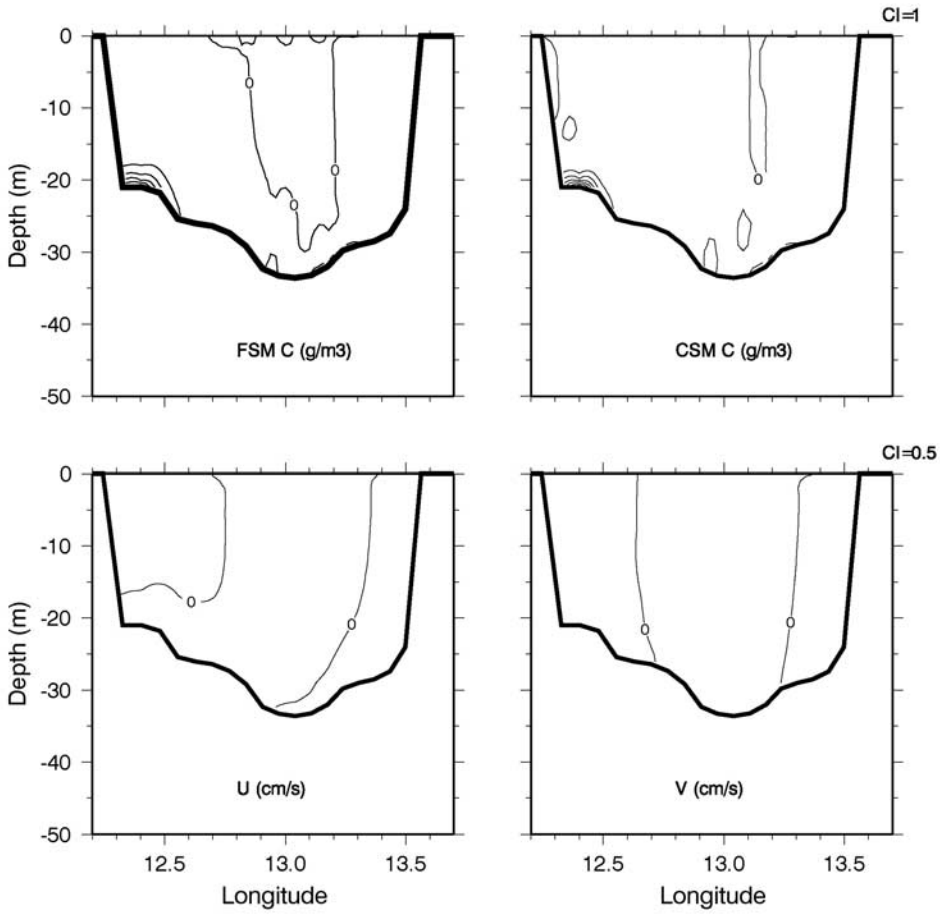

Figure 10. Difference in model simulated sediment concentrations and current velocity at the cross-section N between two Bora wind-forcing experiments with the uniform and the SMB wave fields, respectively.

4.1.7. Po River Plume With Stronger Bora Wind Stress, and Sverdrup-Munk-Bretschneider Wave Fields

[51] In previous process study experiments concerning wind forcing (Experiments 2–5), the wind stresses of both Bora and Scirocco regimes are assumed to have equal magnitude (0.1 N m^{-2}). However, in the Northern Adriatic winter Bora events generally present stronger winds than summer Scirocco. In order to test the sensitivity of sediment fluxes to a stronger Bora wind, Experiment 5 is repeated with a doubled Bora wind stress (0.2 N m^{-2}). The SMB wave height and period in the Northern Adriatic Sea are increased from 0.53 m and 2.7 s at the eastern coast to 2.3 m and 6 s on the western shore respectively. Due to stronger wind-driven currents as well as the larger wave height and period, the southward total sediment transport predicted by this experiment is increased to 610 kg s^{-1} at the cross-section N and 1518 kg s^{-1} at the cross-section S. This experiment shows that stronger Bora winds can generate larger southward sediment transport at the cross-section N than Scirocco wind forcing with its wave resuspension (Table 2).

4.2. Realistic Forcing Experiment

[52] Finally we carried out a realistic simulation for November 1994. The model was driven by the European Centre for Medium Range Weather Forecast (ECMWF) 6-hours analysis fields for air temperature, dew point temperature at 2 m, and wind velocity at 10 m. Monthly mean clouds from COADS (Comprehensive Ocean Atmosphere Data Set) were used as well as climatological precipitation data from *Legates and Willmott* [1990]. These different parameters were used because neither clouds nor precipitation values from ECMWF analyses are good enough to be used in bulk parameterization. The novel model implementation here consists of the development of the air-sea interface physics of the model [*Maggiore et al.*, 1998] which allows to compute heat fluxes in an interactive way. All the rivers, clustered into 13 sources, were implemented in the model, all along the Adriatic coastlines. The most important is the Po which was set at daily flow rate values for our computation. The other river runoffs were set equal to their seasonal average runoff values for lack of higher frequency data. Open boundary conditions in the Ionian Sea along a latitudinal boundary located at 39°N were nested within a large-scale model of the Mediterranean Sea [*Pinardi and Masetti*, 2000].

[53] The ASGCM with above configuration was run continuously from 1992 to 1994. The SSM transport model was coupled to this ASGCM run from October 31 ASGCM integration. The sediment concentration fields were initial-

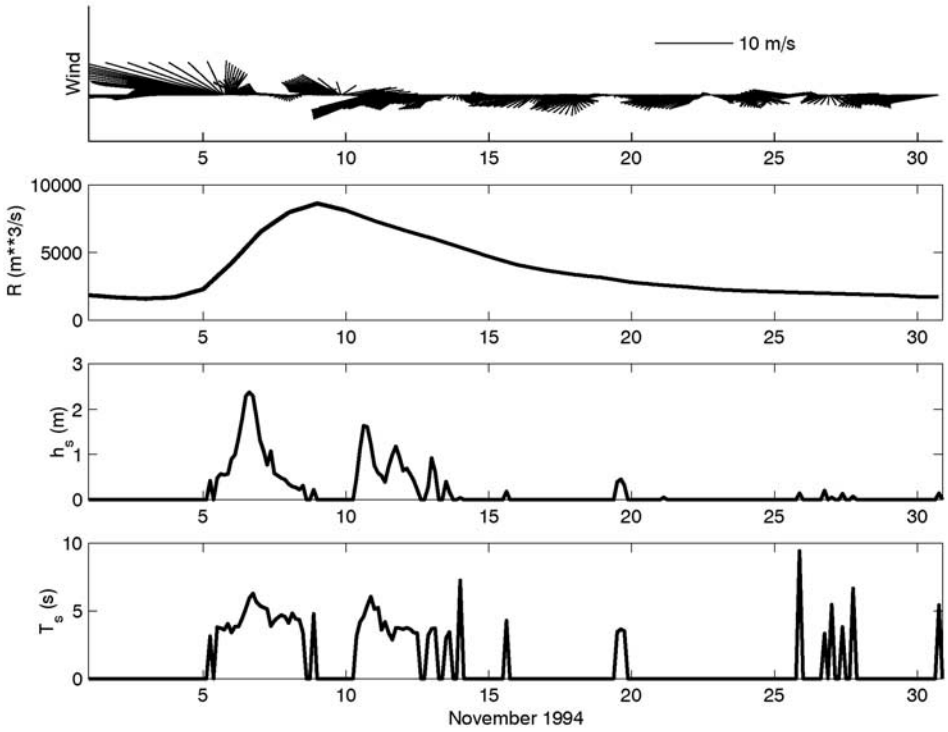

Figure 11. Forcing functions of the realistic forcing experiment for November 1994. (top to bottom) Northern Adriatic Sea surface area averaged wind vector on a conventional geographical coordinate system, Po River runoff, significant wave height and wave period observed south of Venice Lagoon.

ized by the quasi-steady-state sediment plume simulated by the winter Po River buoyancy forcing experiment shown in Figure 3, approximating the Po River-induced equilibrium sediment distribution for winter season. The observed November 1994 surface wave data was also used for wave current interaction.

[54] The forcing functions of the wind stress, the Po River runoff and wave data are shown in Figure 11 for November 1994. The wind vectors were surface area averaged over the Northern Adriatic Sea, and on the conventional geographical coordinate system. Wave data are at 3-hour intervals, and were obtained from an oceanographic station outside of Venice Lagoon [*Cavaleri et al.*, 1997]. We used these wave data uniformly for the entire Northern Adriatic Sea. This approximation should not alter our conclusions significantly as the wave data reasonably represent the wave conditions on the western shore of the Northern Adriatic Sea [*Cavaleri et al.*, 1989]. It is that area where the spatial variability in the wave fields had maximum effects on the sediment distributions and fluxes as already shown previously. It can also be seen in Figure 11 that the onshore southwest winds are small and should not generate major wave resuspension of sediments on the eastern shore during this period.

[55] Two strong wind events can be noted with wind speeds more than 10 m s^{-1}. The first is a Scirocco event occurred around November 5 and the latter was a Bora event around November 11. After November 5 the Po River runoff increased fourfold of its flow rate, reaching approximately 9000 m^3 s^{-1} for 2–3 days. Relating to two strong wind events, wave heights reached maximum values of more than 1 m with wave period about 5 s on November 6 and 10.

[56] Figure 12 shows four examples of model simulated FSM and CSM distributions and horizontal fluxes at the cross-section S on November 5, 6, 11 and 26. A Scirocco storm on November 5 produced northward coastal fluxes at surface (Figure 12a). Influenced by the Po River induced FSM plume of high concentration, the FSM flux is strong near the Po River delta. A returning bottom flow formed a southward flux, which is an analogy to the one found in Figure 7 that was caused by a stronger subsurface flow in that case. As the section S was not affected by CSM plume, both CSM concentration and flux are low. On November 6, strong wave resuspension coupled with the coastal currents driven by the combined effects of the Po River plume and the wind stress produced strong northward flux at the bottom on the western shelf (Figure 12b). A stronger CSM horizontal flux was also simulated there. A weaker surface plume is also noticeable that advected sediments to the south. This structure of the sediment fluxes underlies the processes described early in Figure 9.

[57] On November 11, a significant Bora wind event enhanced the Po River plume, and the vertical distribution of the southward coastal current became more uniform with depth (Figure 12c). A band of southward sediment flux similar to Figure 6 occupied the entire water column with a maximum value at the surface. FSM concentration and flux have higher values than those of the CSM. The relative high bottom FSM concentration is the recollection of the previous wave suspension event. This twin peak distribution of sediments has been observed by the turbidity measurements

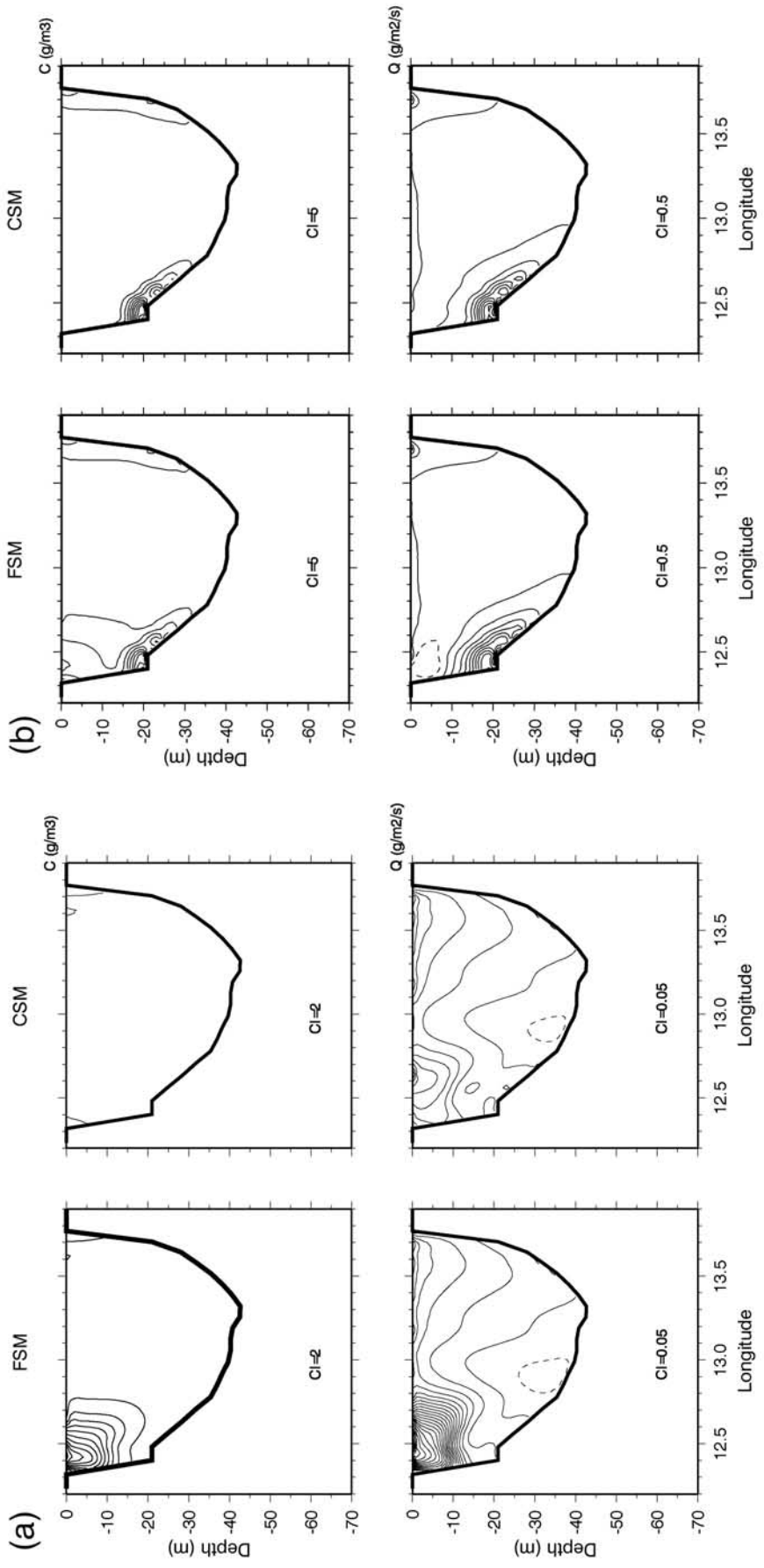

Figure 12. (top) Model simulated sediment concentrations and (bottom) fluxes at cross-section S by November 94 realistic forcing experiment. (a) November 5, (b) November 6, (c) November 11, and (d) November 26. Southward fluxes are in negative values denoted by the dashed lines.

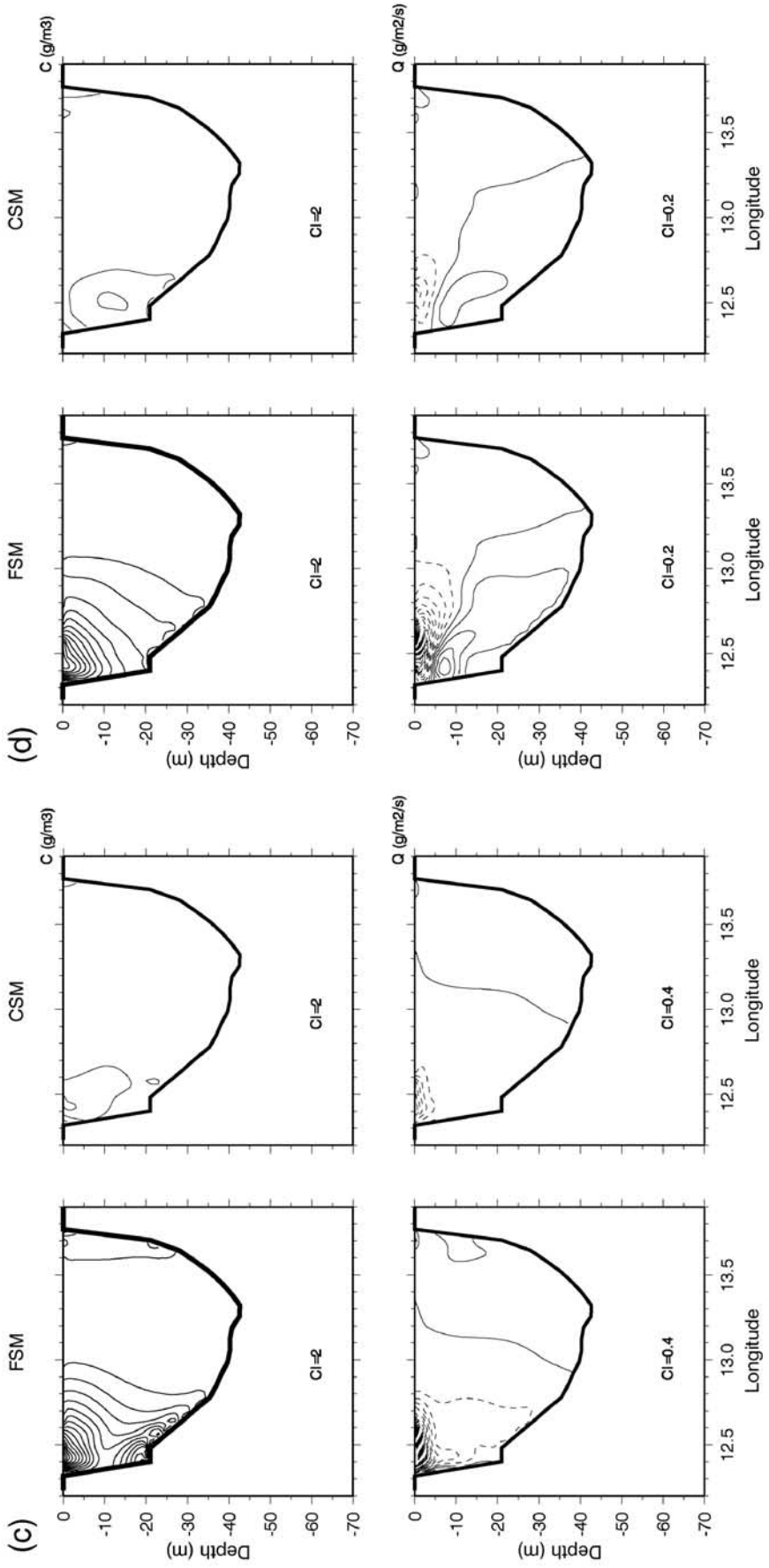

Figure 12. (continued)

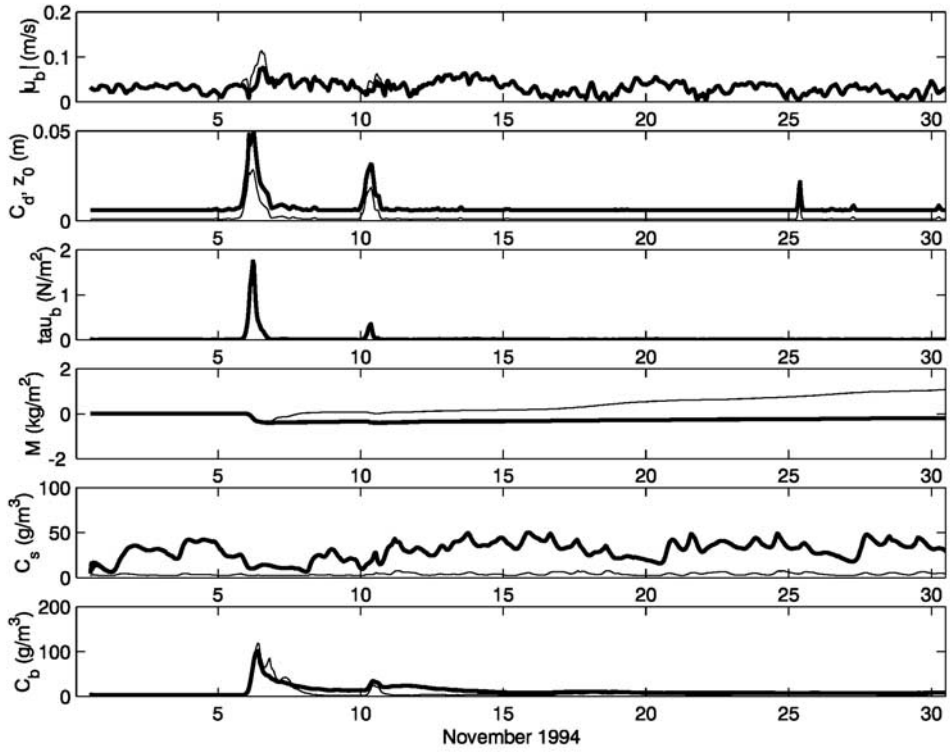

Figure 13. Model simulated hourly time series of BBL hydrodynamics properties, bed load, and sediment concentrations by realistic forcing experiment at station S1. (top to bottom) Bottom mean current $|\boldsymbol{u}_b|$ simulated with (thick line) and without (thin line) wave current interaction; bottom roughness z_0 (thin line) and drag coefficient C_d (thick line); bottom stress τ_b; bed load M for FSM (thick line) and CSM (thin line); surface sediment concentration C_s for FSM (thick line) and CSM (thin line); bottom sediment concentration C_b for FSM (thick line) and CSM (thin line).

taken at station S1 south of Po delta during October 1995 and January 1996 cruises (M. Giani, personal communication, 1999). The sediment distributions and fluxes on November 26 are shown in Figure 12d. It is a period when both wind and waves are weak. The dynamics is then dominated by the Po River plume as studied previously (Figures 3 and 4). The two-layer structure of the fluxes clearly elucidated the baroclinic coastal flow, which produced a southward maximum flux at the surface offshore and a northward maximum flux at a depth of 10 m nearshore. Influenced by Po River plume, FSM concentration and horizontal flux had higher values than those of the CSM.

[58] To further investigate the response of sediments to wave resuspension and the effect of the wave current interaction on BBL hydrodynamics, hourly time series of BBL properties, bed load and surface and bottom sediment concentrations are assessed for stations S1, S2 and S3 (Figure 1b). Bed load is the time integration of the bottom sediment flux S defined by equation (8). Station S1 is located at a water depth of 20 m adjacent to Po River delta. As shown in Figure 13, large wave events increased the bottom roughness z_0 from 0.001 m to a maximum of 0.028 m. This in turn increased the bottom drag coefficient C_d from 0.006 to a maximum value of 0.049, and the wave-driven bottom stress became at least one order of magnitude larger than those produced by the mean current. It should be noted that an increase in C_d due to wave current interaction caused a bottom current reduction by up to 30%. For comparison the bottom current speed simulated by a November 1994 run without waves is also shown in the figure. This result is in agreement with *Hearn and Hunter* [1987], *Signell et al.* [1990] and *Hearn* [1999]. The former authors found a bottom stress parameterized by the traditional quadratic drag law overestimated the bottom currents in shallow coral lagoons where waves are significant, and derived a linear bottom drag coefficient in favor of the quadratic parameterization. While a complete assessment of the wave effect on the large-scale dynamics is beyond the scope of this study, it is demonstrated here that wave current interaction can considerably modified BBL hydrodynamics, thus affect sediment fluxes and distributions in the shallow waters.

[59] Sediment response to the waves can be further examined by observing the variability in bed load and sediment concentrations. The November 6 wave event resulted in bed load erosion, and an increase of bottom FSM and CSM concentrations. This event was followed by a smaller resuspension episode on November 10. In contrast, the surface sediment concentrations were determined by Po River plume and wind forcing and the values remained relatively constant without obvious effect of the wave resuspension.

[60] Station S2 is located on the Italian continental shelf further south of Po River delta. As station S2 has an equal depth to station S1, the waves had the similar effect on the

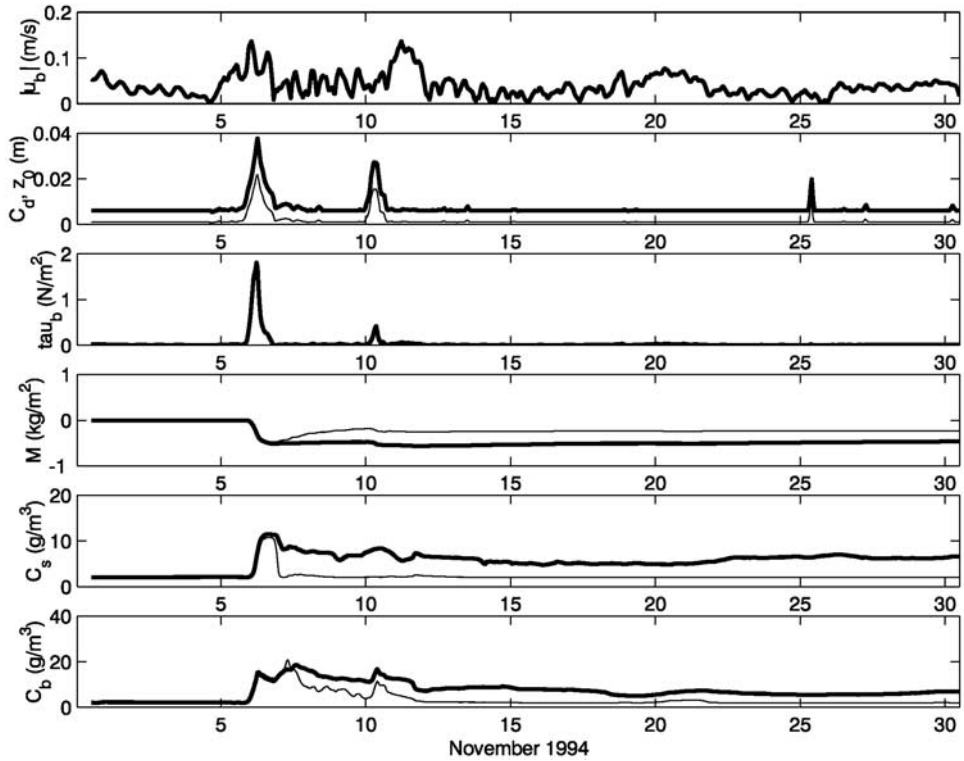

Figure 14. Same as Figure 13 but for station S2.

BBL hydrodynamics there (Figure 14). However, certain difference in sediment distributions can be identified between two stations. As buoyancy induced stratification decreases away from the river sources, vertical eddy diffusivity value increases. The depth averaged eddy viscosity was 0.002 $m^2\ s^{-1}$ and 0.015 $m^2\ s^{-1}$ at stations S1 and S2 respectively. Figure 15 shows salinity, vertical eddy diffusivity and both FSM and CSM profiles on November 6 at both stations. At station S1, the river plume stratified the water column by salinity, and suppressed the vertical eddy diffusivity in the water column. The sediments suspended by the waves were confined within a bottom layer of 5 m. Station S2 was less affected by the river plume, and the salinity there was more well mixed. Stronger turbulence intensity was able to produce upward sediment fluxes that resulted in well mixed FSM and CSM concentration profiles.

[61] It should be noted here that an upward FSM flux at station S2 was in part driven by a coastal upwelling event due to Scirocco winds on November 6. Figure 16 shows the model simulated vertical sediment fluxes at the cross-section W (Figure 1b) on the same day. While positive FSM fluxes due to vertical mixing can be observed, the wind-driven upwelling exceeded the FSM settling and produced upward fluxes near the coast. As the CSM settling velocity is one order of magnitude larger than the vertical water velocity on the western shelf, the vertical advection produced downward CSM fluxes there. However, the vertical diffusion had a dominant influence on the vertical CSM fluxes, thus resulted in net upward CSM fluxes in the water column. The topographic induced upwelling is also evident near the basin center, and causes upward transport of both FSM and CSM there.

[62] Station S3 is located in the deep part of the Northern Adriatic Sea, where waves caused minimal sediment resuspension on November 6. As the location is beyond the offshore extension of the Po River sediment plume both with and without the influence of wind forcing, sediment concentrations remained largely unchanged from their initial background values (figure not shown).

[63] We finally note that the wave-driven sediment resuspension caused bed load erosion at station S1 and S2 due to two large wave events of November 6 and 10. Strong lateral advection and deposition of the coarse sediments discharged from the Po River resulted in a net CSM deposition at station S1 by the end of November 1994.

5. Discussion and Conclusions

[64] A coupled ASGCM and sediment transport model was used to study the dynamics of the SSM transport and resuspension in the Northern Adriatic Sea. The BBL was resolved by the coupled model with high vertical resolution, and the mechanism of the wave current interaction was also represented in the model.

[65] The process study experiments assessed the sediment transport processes that affect the sediment distributions and fluxes under the separate and concomitant forcing of the Po River plume, the wind stress and the surface waves. Under the Po River plume forcing, there is a large northward sediment flux at cross-section N and a smaller southward flux at the cross-section S. Most of these sediment fluxes at both cross-sections were mostly contributed by the fine sediment materials discharged from the Po River. The values of these fluxes generally increase with the river runoff rates.

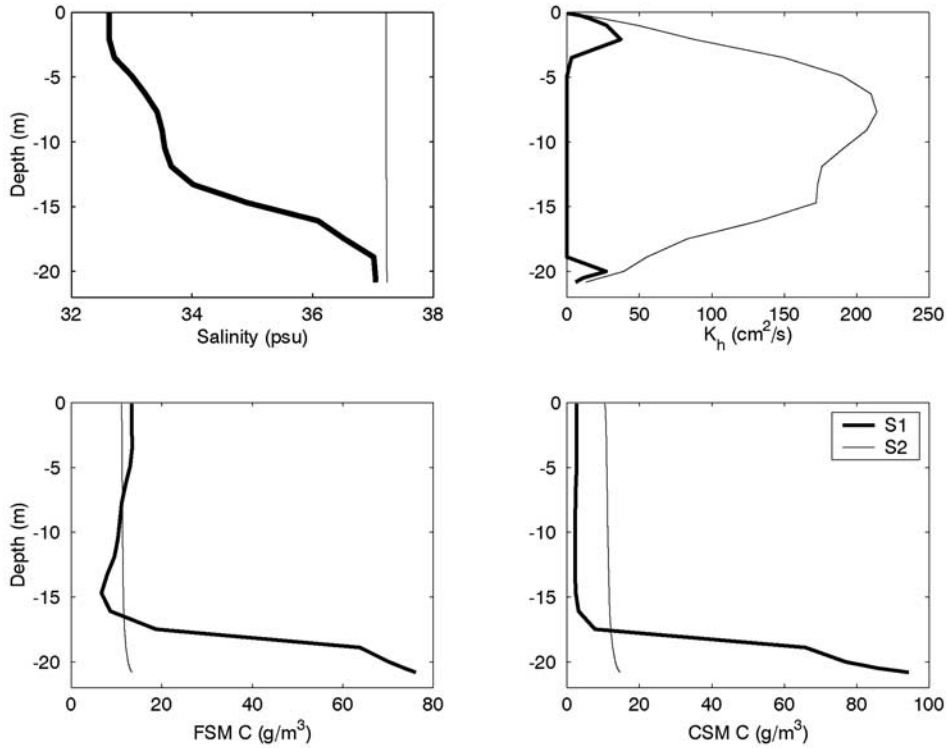

Figure 15. Model simulated depth profiles for salinity, vertical eddy diffusivity K_h and sediment concentration C at station S1 (thick line) and S2 (thin line) on November 6, 1994.

However, a reduced river plume can also increase the northward flux due to a weakened anticyclonic plume gyre situated north of the delta. The combined effect of Po River plume and wind stress forcing reversed or significantly reduced northward sediment fluxes at cross-section N for Bora and Scirocco winds respectively. Wind-forcing also increased southward fluxes at the cross-section S.

[66] When wave resuspension was considered, the sediment fluxes predicted by previous experiments are strengthened. Scirocco waves that have longer period give much stronger effect on sediment distributions and fluxes. The CSM contribution to total sediment fluxes became equally or more important than the FSM contribution. The Po River plume-forcing run with Scirocco wave resuspension predicted a northward sediment flux, mostly contributed by CSM due to its high bottom concentration at cross-section S. This is an anomalous direction for sediment fluxes at this location. Moreover, the same run also predicted large northward sediment flux at cross-section N.

[67] The important forcings that resulted in significant horizontal sediment fluxes at cross-section N and S can be synthesized as follows. The largest northward sediment fluxes at cross-section N and S occurred under the forcing by the Po River plume with Scirocco wave resuspension. The largest southward sediment flux at the cross-section S was due to the combined effect of Po River plume and Bora wind forcing with Bora wave resuspension. When a more realistic Bora wave field generated by the SMB wave model was introduced, the sediment flux at the cross-section S was reduced by 2%.

[68] Vertical sediment fluxes were two to three orders of magnitude smaller than the horizontal sediment fluxes, and were determined by vertical advection (including sediment settling) and vertical diffusion. Our study has shown that vertical water movements such as upwelling or downwelling can significantly affect the vertical FSM flux. As the settling velocity for the CSM was an order of magnitude larger than the vertical velocity of the water particles found in the region, the vertical CSM flux was mostly negative (downward) when the vertical mixing was weak. The vertical diffusion became important and resulted in positive (upward) vertical sediment fluxes when bottom resuspension was strong.

[69] The November 1994 simulation of the SSM transport was run with realistic atmospheric fluxes, river runoffs and wave forcings. Strong wind events, Po River runoffs and significant waves were observed during this month, and covered the full ranges of the forcing conditions important to sediment transport processes for the region, as reviewed by the process studies. The model simulated sediment fluxes and distributions varied considerably, and the variability elucidated the relative importance of Po River plume, wind stress, and surface wave forcings in determining sediment fluxes and distributions in the Northern Adriatic.

[70] In order to demonstrate the sediment grading processes observed in the Northern Adriatic Sea, the November 1994 monthly mean depth averaged sediment distributions and horizontal sediment fluxes are shown in Figure 17. Stronger southward FSM flux south of Po River delta resulted in a fine sediment coastal plume extended as far as the southern end of the basin. In contrast, there was a much smaller southward transport of CSM in the most of western coastal regions, and the CSM plume was confined near the Po River sources. Figure 17 also shows there was a FSM flux in the northern coast of the Adriatic Sea trans-

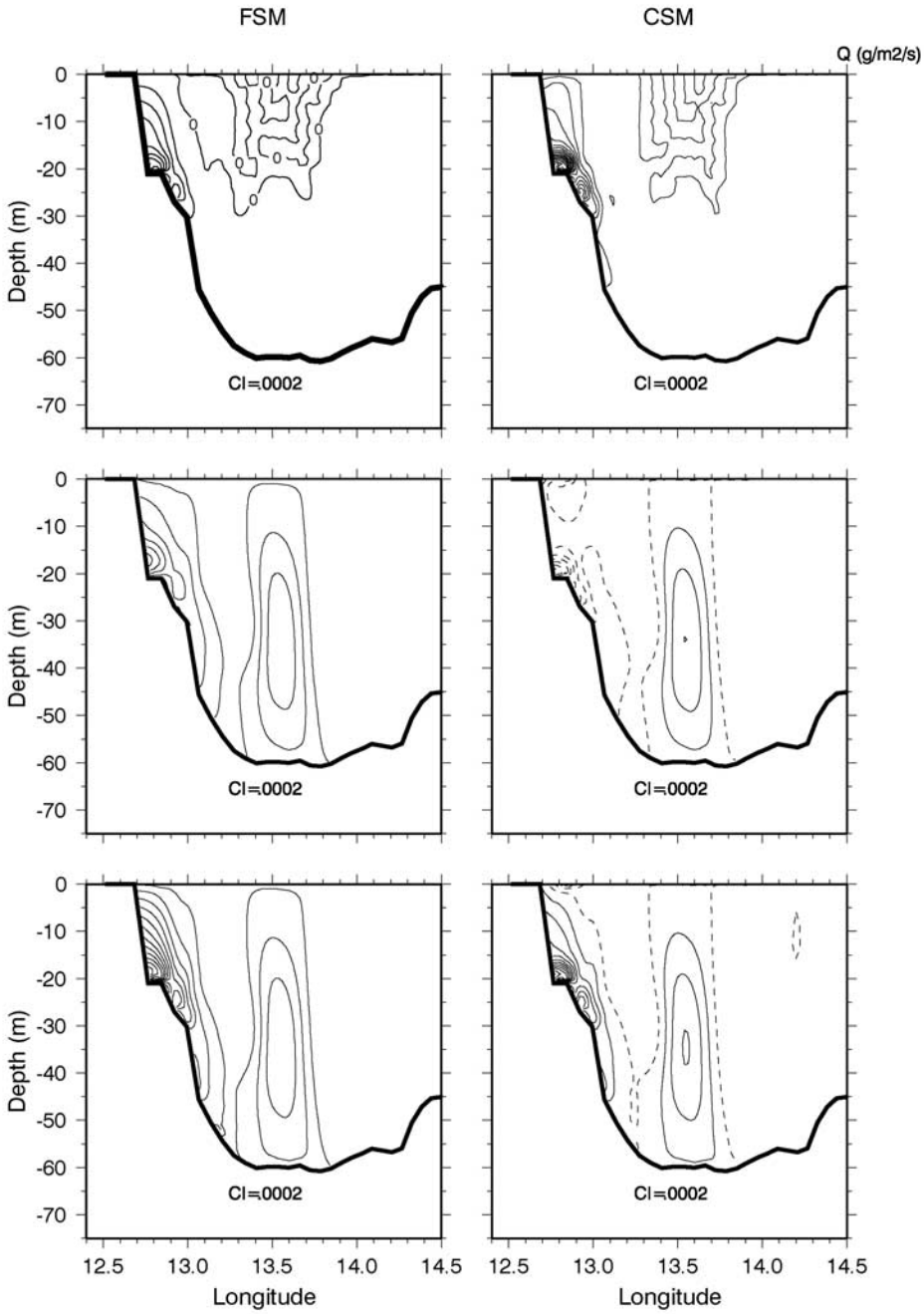

Figure 16. Model simulated vertical sediment fluxes at cross-section W on November 6, 1994. (top) $-K_h\frac{\partial C}{\partial z}$; (middle) $(w + w_s)C$; (bottom) $(w + w_s)C - K_h\frac{\partial C}{\partial z}$. Downward fluxes are in negative values, denoted by the dashed lines.

porting the FSM eastward. Above fine and coarse sediment distribution patterns are consistent with the sediment sorting processes discussed by *Brambati et al.* [1973].

[71] By means of wave current interaction, this study has shown that wave-driven sediment resuspension is an important sediment resuspension mechanism in the shallow western shore of the Northern Adriatic Sea, and contributes significantly to the sediment distributions and fluxes. The study also revealed that the plume-induced stratification prevented vertical mixing of wave resuspended sediments from the bottom to the surface.

[72] In this study we have assumed the SSM has no effects on the water density due to its small concentration values. To validate this assumption, the realistic forcing experiment was repeated with a new parameterization of the bottom drag coefficient according to *Wang* [2002]:

$$C_d = \left[\frac{1}{\kappa/(1 + AR_f)}\ln(H + z_b)/z_0\right]^{-2} \tag{13}$$

In the above, the effect of the sediment-induced stratification on the bottom stress is considered by a stability

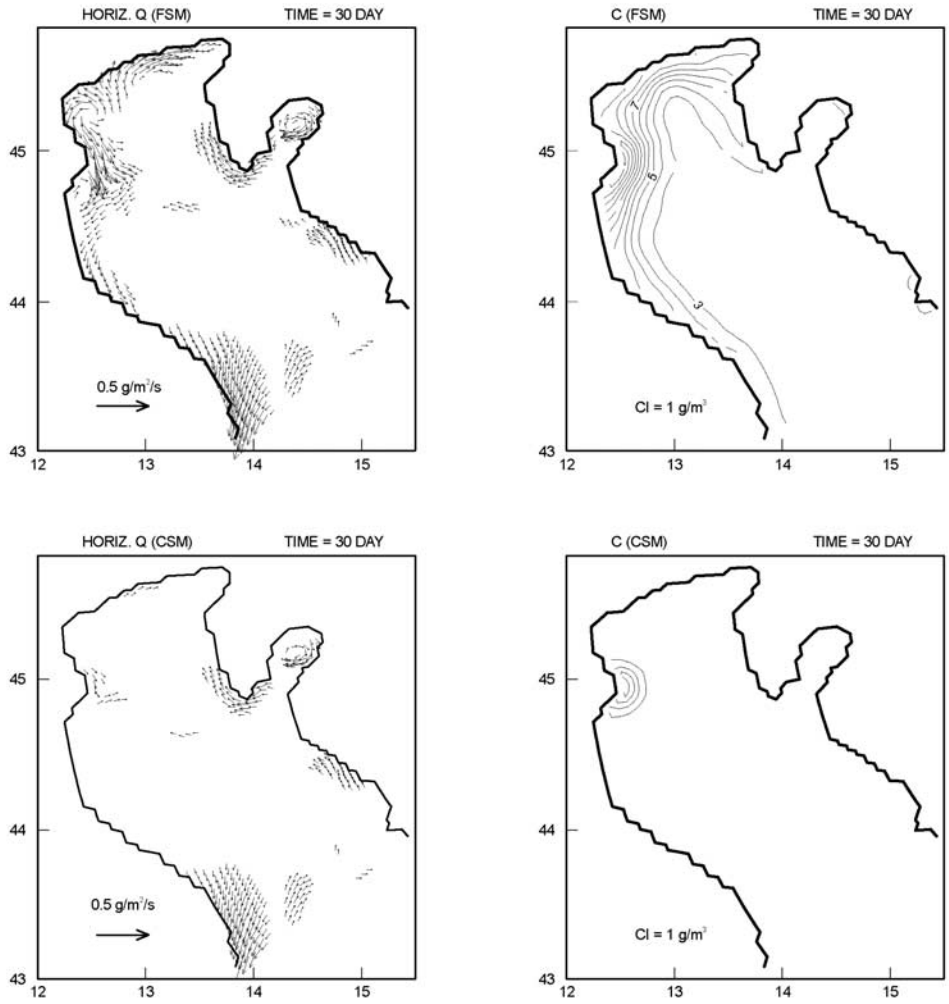

Figure 17. Model simulated monthly mean depth averaged sediment fluxes and concentrations from November 1994 realistic forcing experiment. Vectors less than 10% of maximum fluxes are not plotted.

function $(1 + AR_f)^{-1}$, where A is an empirical constant and R_f is a flux Richardson number computed by the Mellor-Yamada turbulent closure scheme. *Adams and Weatherly* [1981] determined $A = 5.5$ for a sediment-laden oceanic bottom boundary layer. Furthermore, the SSM concentration and the water density were coupled with a volumetric relation also used by *Wang* [2002].

[73] Figure 18 shows the model predicted bottom drag coefficient at station S1 where the bottom C is predicted to be largest (Figure 13). During the wave resuspension events, the drag coefficient values are intermittently reduced due to stronger SSM concentrations in the BBL, but they are still in the same order of magnitude as those predicted by equation (1c). In general, the drag coefficient values predicted by equations (13) and (1c) are in good agreement for the entire modeling period. Therefore, the coupling of the SSM concentrations and the water density has negligible effects on the concentrations and currents at the station S1

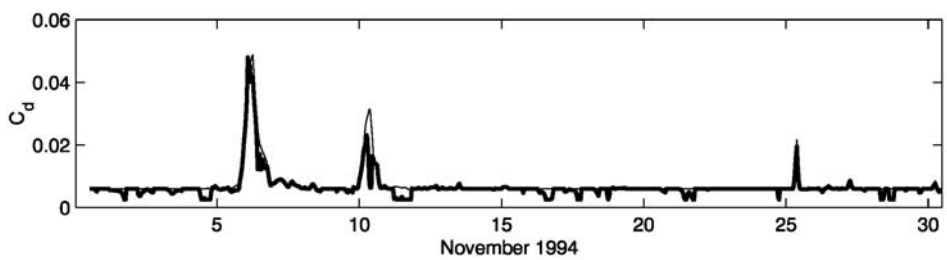

Figure 18. Model simulated hourly time series of the bottom drag coefficient C_d by equation (13) (thick line) and equation (1c) (thin line) at the station S1.

(figure not shown). Similarly, no effects on concentrations and currents are predicted at the other stations, as the SSM concentrations are even lower there.

[74] From this work we presented the complex features of the Northern Adriatic Sea sediment distributions and fluxes under various forcing conditions experienced in the region. Previous researchers have observed some of these features, such as the sediment grain sorting processes by coastal currents and the twin peak distribution of sediments in the water column near Po River delta. The limited model data comparison offers some promising confidence to provide important information needed for an integrated coastal management system and data acquisition. For instance SSM concentrations strongly affect the light penetration properties, especially in shelf seas. If an ecosystem model could be coupled with our prediction of the SSM distributions and fluxes in the water column, a more accurate representation of the primary production seasonal cycles may result.

Appendix A: Transformation of the SSM Settling Velocity w_s Into a σ -Coordinate System

[75] If x', y', σ are coordinates in a σ -coordinate system, the transformation is:

$$x' = x, y' = y, \sigma = \frac{z-\eta}{D} \tag{A1}$$

where x,y,z are the conventional Cartesian coordinates, and $D(t,x,y) = H(x,y) + \eta(t,x,y)$. Here $H(x,y)$ is the bottom topography, $\eta(t,x,y)$ is the surface elevation.

[76] The transformed vertical velocity in σ -coordinate system is

$$w' = w - u\left(\sigma\frac{\partial D}{\partial x} + \frac{\partial \eta}{\partial x}\right) - v\left(\sigma\frac{\partial D}{\partial y} + \frac{\partial \eta}{\partial y}\right) - \sigma\frac{\partial D}{\partial t} - \frac{\partial \eta}{\partial t}. \tag{A2}$$

[77] As the SSM particle velocity only differs to the water velocity (u,v,w) by sediment settling velocity w_s in the vertical direction in the conventional Cartesian coordinate system, therefore

$$u_{ssm} = u,\ v_{ssm} = v,\ w_{ssm} = w + w_s \tag{A3}$$

where $(u_{ssm},v_{ssm},w_{ssm})$ are the SSM particle velocity.

[78] Substituting (A3) into (A2), we have the SSM vertical velocity in σ -coordinate system as

$$w'_{ssm} = w + w_s - u\left(\sigma\frac{\partial D}{\partial x} + \frac{\partial \eta}{\partial x}\right) - v\left(\sigma\frac{\partial D}{\partial y} + \frac{\partial \eta}{\partial y}\right) - \sigma\frac{\partial D}{\partial t} - \frac{\partial \eta}{\partial t}. \tag{A4}$$

[79] Using (A2) and (A4), we have

$$w'_{ssm} = \omega + w_s. \tag{A5}$$

[80] **Acknowledgments.** Authors wish to thank J. Ribbe for providing the original sediment transport modeling algorithm, A. Maggiore, E. Demirov, M. Zavatarelli, M. Frigniani and F. Frascari for constructive discussions during the project, and L. Calvaleri for providing wave data. X.H. Wang was supported by the 1999 UNSW Special Study Program and the "Progetto Ambiente Mediteraneo" funded by an ENEA-MURST Program Agreement. N. Pinardi was supported by the EU Project MAS3-CT98-0171, Mediterranean Forecasting System Pilot Project.

References

Adams, C. E., Jr., and G. L. Weatherly, Some effects of suspended sediment stratification on an oceanic bottom boundary layer, *J. Geophys. Res.*, *86*, 4161–4172, 1981.

Ariathurai, R., and R. B. Krone, Mathematical modelling of sediment transport in estuaries, in *Estuarine Processes*, vol. II, edited by M. Wiley, pp. 98–106, Academic, San Diego, Calif., 1976.

Artegiani, A., D. Bregant, E. Paschini, N. Pinardi, F. Raicich, and A. Russo, The Adriatic Sea general circulation, I, Air-sea interactions and water mass structure, *J. Phys. Oceanogr.*, *27*, 1492–1514, 1997a.

Artegiani, A., D. Bregant, E. Paschini, N. Pinardi, F. Raicich, and A. Russo, The Adriatic Sea general circulation, II, Baroclinic circulation structure, *J. Phys. Oceanogr.*, *27*, 1515–1532, 1997b.

Blumberg, A. F., and G. L. Mellor, A description of a three-dimensional coastal ocean circulation model, in *Three-Dimensional Models of Marine and Estuarine Dynamics*, *Elsevier Oceanogr. Ser.*, vol. 45, edited by J. C. J. Nihoul and B. M. Jamart, pp, 55–88, Elsevier Sci., New York, 1987.

Brambati, A., D. Bregant, G. Lenardon, and D. Stolfa, Transport and sedimentation in the Adriatic Sea, *Publ. 20*, 60 pp., Museo Friulano di Storia Nat., Udine, Italy, 1973.

Bretschneider, C. L., Forecasting relations for wave generation, *Look Lab Hawaii*, *1*(3), 1970.

Cavaleri, L., and L. Bertotti, In search of the correct wind and wave fields in a minor basin, *Mon. Weather Rev.*, *125*, 1964–1975, 1997.

Cavaleri, L., L. Bertotti, and P. Liobello, Shallow water application of the third-generation WAM wave model, *J. Geophys. Res.*, *94*, 8111–8124, 1989.

Cavaleri, L., S. Curiotto, A. Mazzoldi, and M. Pavanati, Long-term directional wave recording in the Northern Adriatic Sea, *Nouvo Cimento C*, *20*, 103–110, 1997.

Chao, S.-Y., Hyperpycnal and buoyant plumes from a sediment-laden river, *J. Geophys. Res.*, *103*, 3067–3082, 1998.

Clark, S., and A. J. Elliot, Modelling suspended sediment concentration in the Firth of Forth, *Estuarine Coastal Shelf Sci.*, *47*, 235–250, 1998.

Eidsvik, K. J., Parameterization of wave effects upon large-scale bottom boundary layer flow, *Cont. Shelf Res.*, *13*, 903–918, 1993.

Fohrmann, H., J. O. Backhaus, F. Laume, and J. Rumohr, Sediments in bottom-arrested gravity plumes: numerical case studies, *J. Phys. Oceanogr.*, *28*, 2250–2274, 1998.

Frascari, F., M. Frignani, S. Guerzoni, and M. Ravaioli, Sediments and pollution in the Northern Adriatic Sea, *Ann. N. Y. Acad. Sci.*, *534*, 1000–1020, 1988.

Giordani, P., D. E. Hammond, W. M. Berelson, G. Montanari, R. Poletti, A. Milandri, M. Frignani, L. Langone, M. Ravailoi, G. Rovatti, and E. Rabbi, Benthic fluxes and nutrient budgets for sediments in the Northern Adriatic Sea: Burial and recycling efficiencies, *Sci. Total Environ., Suppl.*, 251–275, 1992.

Grant, W. D., and O. S. Madsen, Combined wave and current interaction with a rough bottom, *J. Geophys. Res.*, *84*, 1797–1808, 1979.

Grant, W. D., and O. S. Madsen, The continental-shelf bottom boundary layer, *Annu. Rev. Fluid Mech.*, *18*, 265–305, 1986.

Hearn, C. J., Wave-breaking hydrodynamics within coral reef systems and the effect of changing relative sea level, *J. Geophys. Res.*, *104*, 30,007–30,020, 1999.

Hearn, C. J., and J. R. Hunter, Modelling wind-driven flow in shallow systems on the southwest Australian coast, in *Numerical Modelling: Applications to Marine Systems*, edited by J. Noye, pp. 47–58, Elsevier Sci., New York, 1987.

Hendershott, M. C., and P. Rizzoli, The winter circulation of the Adriatic Sea, *Deep Sea Res.*, *23*, 353–370, 1976.

Jewell, P. W., R. F. Stallard, and G. L. Mellor, Numerical studies of bottom shear stress and sediment distribution on the Amazon Continental Shelf, *J. Sed. Petrol.*, *63*, 734–745, 1993.

Kampf, J., J. O. Backhaus, and H. Fohrmann, Sediment-induced slope convection: Two-dimensional numerical case studies, *J. Geophys. Res.*, *104*, 20,509–20,522, 1999.

Kourafalou, V. H., Process studies on the Po River plume, North Adriatic Sea, *J. Geophys. Res.*, *104*, 29,963–29,985, 1999.

Legates, D. R., and C. J. Willmott, Mean seasonal and spatial variability in gauge-corrected, global precipitation, *Int. J. Climatol.*, *10*, 111–127, 1990.

Lou, J., D. J. Schwab, D. Belesky, and N. Hawley, A model of sediment resuspension and transport dynamics in southern Lake Michigan, *J. Geophys. Res.*, *105*, 6591–6610, 2000.

Maggiore, A., M. Zavatarelli, M. G. Angelucci, and N. Pinardi, Surface heat and water fluxes in the Adriatic Sea: Seasonal and interannual variability, *Phys. Chem. Earth*, *23*(5–6), 561–567, 1998.

Malanotte-Rizzoli, P., and A. Bergamasco, The dynamics of the coastal regions of the Northern Adriatic Sea, *J. Phys. Oceanogr.*, *13*, 1105–1130, 1983.

Mellor, G. L., User's guide for a three-dimensional, primitive equation numerical ocean model, report, 35 pp., Program in Atmos. and Ocean. Sci., Princeton Univ., Princeton, N. J., 1998.

Mellor, G. L., and X. H. Wang, Pressure compensation and the bottom boundary layer, *J. Phys. Oceanogr.*, *26*, 2214–2222, 1996.

Pinardi, N., and E. Masetti, Variability of the large-scale general circulation of the Mediterranean Sea from observations and modeling, *Palaeogeogr. Palaeoclimatol. Paleoceanogr.*, *158*, 153–173, 2000.

Poulain, P.-M., Adriatic Sea surface circulation as derived from drifter data between 1990 and 1999, *J. Mar. Syst.*, *29*, 3–32, 2001.

Raicich, F., On the fresh water balance of the Adriatic Sea, *J. Mar. Syst.*, *9*, 305–319, 1996.

Ribbe, J., and P. E. Holloway, A model of suspended sediment transport by internal tides, *Cont. Shelf Res.*, *21*, 395–422, 2001.

Signell, R. P., R. C. Beardsley, H. C. Graber, and A. Capotondi, Effect of wave-current interaction on steady wind-driven circulation in narrow, shallow embayment, *J. Geophys. Res.*, *95*, 9671–9678, 1990.

Smagorinsky, J., General circulation experiments with the primitive equations, I, The basic experiment, *Mon. Weather Rev.*, *91*, 99–164, 1963.

Smorlarkiewicz, P. K., A fully multidimensional positive definite advection transport algorithm with small implicit diffusion, *J. Comput. Phys.*, *54*, 325–362, 1984.

Trowbridge, J. H., and G. C. Kineke, Structure and dynamics of fluid muds over the Amazon continental shelf, *J. Geophys. Res.*, *99*, 865–874, 1994.

Vichi, M., N. Pinardi, M. Zavatarelli, G. Matteucci, M. Marcaccio, M. C. Bergamini, and F. Frascari, One-dimensional ecosystem model tests in the Po Prodelta area (Northern Adriatic Sea), *Environ. Model. Software*, *13*, 471–481, 1998.

Wang, X. H., A numerical study of sediment transport in a coastal embayment during a winter storm, *J. Coastal Res.*, *34*, Spec. Issue, 414–427, 2001.

Wang, X. H., Tide-induced sediment resuspension and the bottom boundary layer in an idealized estuary, *J. Phys. Oceanogr.*, *32*, 3113–3131, 2002.

Wang, X. H., and G. Symonds, Coastal embayment circulation due to atmospheric cooling, *J. Geophys. Res.*, *104*, 29,801–29,816, 1999.

Warren, R., and J. Johnsen, Cohesive sediment modelling for coastal lagoons, paper presented at International Colloquium and Exposition on Computer Applications in Coastal and Offshore Engineering (ICE-CA COE'93), Kuala Lumper, Malaysia, June 14–16, 1993.

Zavatarelli, M., and G. L. Mellor, A numerical study of the Mediterranean Sea circulation, *J. Phys. Oceanogr.*, *25*, 1384–1414, 1995.

Zavatarelli, Z., N. Pinardi, V. H. Kourafalou, and A. Maggiore, Diagnostic and prognostic model studies of the Adriatic Sea general circulation: Seasonal variability, *J. Geophys. Res.*, *107*, 3004, doi:10.1029/2000JC000210, 2002.

N. Pinardi, Physics Department, University of Bologna, Viale Berti Pichat 6/2, Bologna, Italy.

X. H. Wang, School of Geography and Oceanography, University College, ADFA, University of New South Wales, Canberra, ACT 2600, Australia. (hua.wang@adfa.edu.au)